REPRINT NO. 26

R62SD55

HYPERSONIC ABLATION

L. STEG and H. LEW

SPACE SCIENCES
LABORATORY

MISSILE AND SPACE DIVISION

GENERAL ELECTRIC

SPACE SCIENCES LABORATORY

AEROPHYSICS SECTION

HYPERSONIC ABLATION

By

L. Steg and H. Lew

Presented at AGARD Hypersonic Conference
TCEA, Rhode-St. Geneva, Belgium
April 3-6, 1962

R62SD55
May, 1962

MISSILE AND SPACE DIVISION

GENERAL ELECTRIC

CONTENTS

ABSTRACT

The severe high enthalpy environment generated by vehicles entering into atmospheres at hypersonic speeds has led to the consideration of material ablation as a means of alleviating the high heat flux.

Refractory material, such as quartz, upon exposure to high enthalpy environment softens, melts, and flows under the influence of gas-shearing action. A fraction of the melt vaporizes and is introduced into the boundary layer. The behavior of this melt is complicated, of course, by body forces due to deceleration and to instability at the liquid-air interface.

In another class of materials such as Teflon, the intermediate liquid phase is not present and sublimation of the solid occurs directly. This type of material sublimes at a low surface temperature and, through a depolymerization process, a monomer is formed which reacts with the environmental constituents of dissociated air species.

At high surface temperatures the plastics, such as those represented by a phenolic resin reinforced with nylon or by a foamed polyurethane, are proven ablators. A thin layer of plastic is affected by the high heat flux due to its low thermal conductivity. Characteristics of the behavior of this class of material are the char layer formed from the depolymerization process within the plastic and the generation of gases represented by methane, hydrogen, etc. Further complication occurs due to the oxidation processes at the surface of the char with the dissociated air species.

Refractory material, as graphite, ablates by the oxidation process and is affected by the mass transfer and heterogeneous reactions at its surface.

It has been demonstrated that these classes of material are useful for the survival of materials in re-entry environment. This survey paper reviews the behavior of these materials from an experimental and theoretical point of view. Some interesting areas for further investigation are pointed out.

HYPERSONIC ABLATION

L. Steg and H. Lew

I. INTRODUCTION

The severe high enthalpy environment generated by re-entry vehicles at hypersonic speeds has led to the consideration of several methods for alleviating the high heat flux. The flight spectrum for various types of re-entry is shown in Figure 1.

Typical re-entry heating cycles appear in Figure 2a, which shows comparative stagnation point heating rates for a re-entry satellite, a high speed re-entry vehicle and a glide vehicle. Heat fluxes for typical ballistic and satellite re-entry vehicles (stagnation point) are shown in Figure 2b.

The three basic types of heat alleviation schemes are the heat sink, forced mass transfer systems (transpiration cooling devices, radiators), and the self-regulating mass transfer systems (ablation).

The use of heat sink materials, which absorb aerodynamic heat through a temperature rise in a non-melting thick skin, has been covered extensively in the literature (5, 6). Alternatively, a thin sheet of heat sink material, backed by insulation, can be designed to re-radiate the aerodynamic heat indicated in Figure 2. The weight of heat sinks sufficiently thick to be self-insulating becomes excessive; the weight of insulation as well as structural and fabrication problems associated with large thin re-radiating structures must be considered in the re-radiation approach.

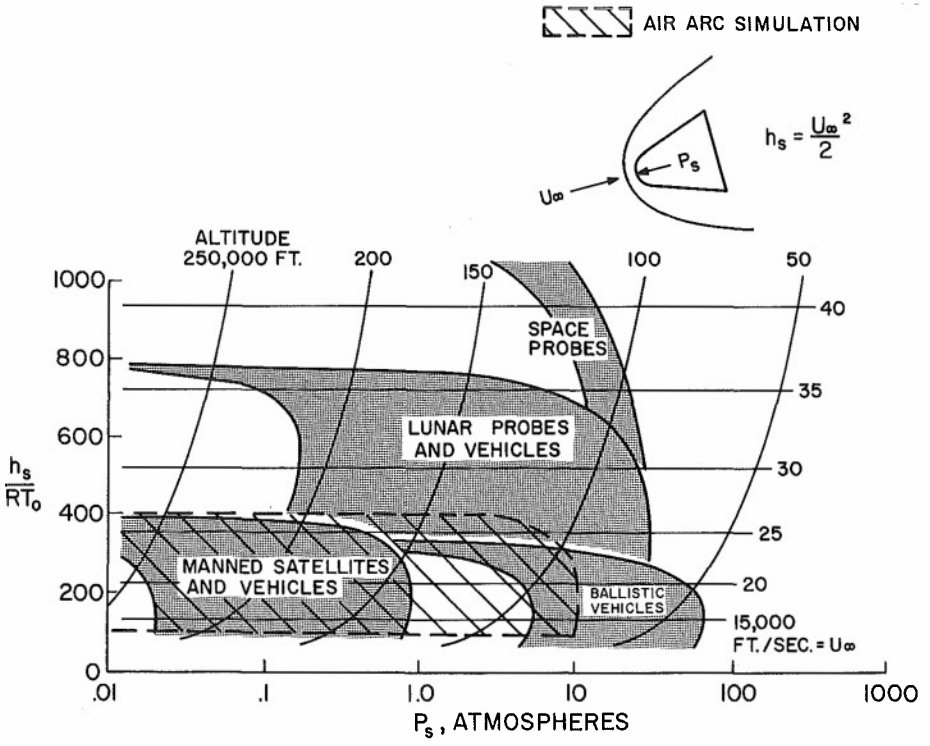

Figure 1. Re-entry Vehicle Flight Spectrum

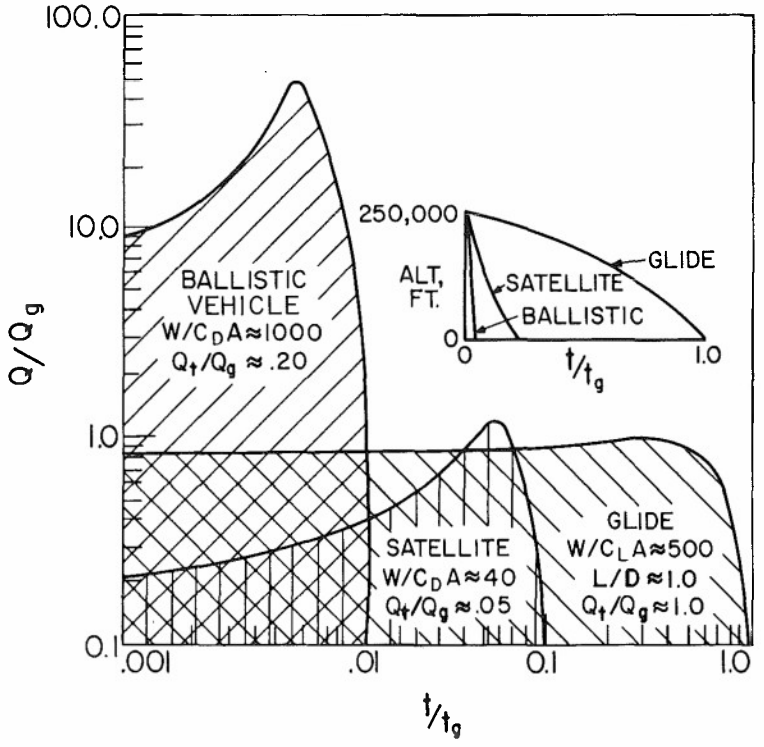

Figure 2a. Typical Re-entry Heating Cycles

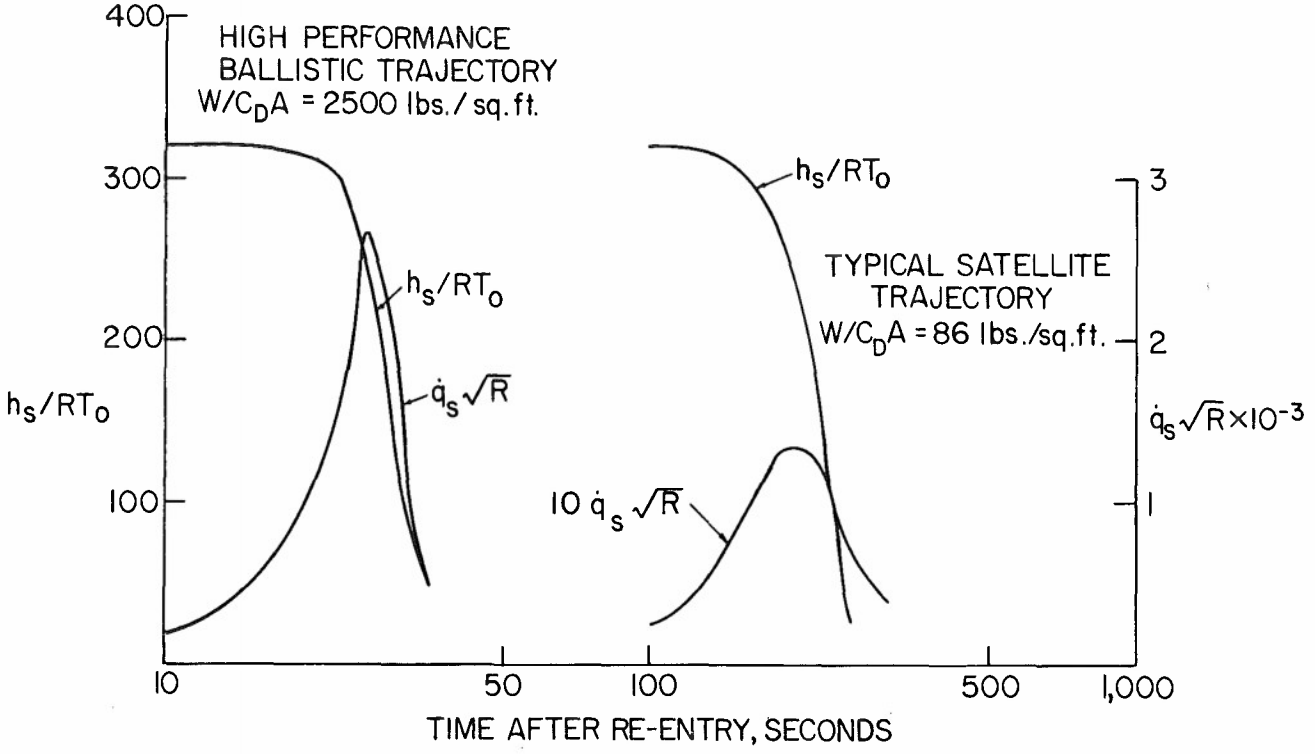

Figure 2b. Aerodynamics Heating Rates

Typical forced mass transfer cooling techniques require relatively small amounts of coolant, approximately one pound of air per square foot of surface to be protected (4); the feasibility of providing reliable permeable materials over the relatively large surface area of interest remains to be demonstrated.

Ablation (refs. 7 to 13, 30, 31, and 32) has proven to be an attractive method for both the thermal protection of high speed re-entry vehicles with their associated high ballistic heat pulse and the longer and less severe heating rates of re-entry satellites.

It is the object of this survey to review some recent work in hypersonic ablation.

Some generally desirable characteristics of ablation materials are as follows:

a. In general, gasification during ablation is desirable. The large amount of gas generated thickens the boundary layer and reduces the rate of heat transfer. Gasification products of low molecular weight enhance this effect because of their larger heat capacity and larger diffusion coefficients.

b. They should have good thermal insulation characteristics so that the ablation process, the loss of structural strength resulting from heating beyond the ablation zone, and the effect of local irregularities during ablation, are confined to the surface.

c. They should have a high resistance to thermal and mechanical shock and be easy to fabricate in large sizes.

Materials of interest and the general approach followed may be grouped as follows:

I Plastics which depolymerize to a gas but do not liquefy, e.g., Teflon. Account will be taken of depolymerization kinetics and combustion with air.

II Materials which sublime and react with the constituents of dissociated air, e.g., graphite. In the theoretical consideration of these materials, it will be assumed that no further homogeneous chemical reactions occur between the products of surface combustion and air.

III Materials which first melt and then vaporize, e.g., glass. Liquid film flow and heat conduction have been determined by the integral method and similarity method at the stagnation point. The properties of the vaporized species are assumed to be the same as air. The effect of mass transfer on heat transfer has been obtained from results for dissociated air.

IV Composite materials such as reinforced plastics or cast un-reinforced resins which pyrolyze and char, e.g., phenolic nylon or epoxy base compositions.

II. PURE GASIFICATION - TEFLON

Teflon was considered for protection from aerodynamic heating as early as ten years ago. Although some supersonic flight tests were performed, they did not yield quantitative information concerning Teflon's ablation properties.

The ablation of Teflon appears to occur by a first order reaction in which the polymer depolymerizes into a monomer (15). The monomer has a very high vapor pressure, so that under most conditions it will flash directly to the vapor. During this process, about 750 Btu/lb are absorbed. If, however, the reaction is carried on at temperatures greater than about 538°C, the viscosity decreases sufficiently as to allow incompletely depolymerized polymers to diffuse through the surface. After being formed, the monomer gas may react with itself to produce unsaturated molecules of higher molecular weight. In the presence of high temperature air, the monomer may also dissociate and burn to form COF_2 or $CO + F_2$.

The first theoretical analysis published (16) considered hypersonic Couette flow over a Teflon wall assumed to be at uniform temperature. It was found that the combustion of the monomer had very little effect on the rate of ablation of Teflon at hypersonic velocities. This conclusion had been reached earlier (17, 18) for the case of a high temperature laminar boundary layer at the stagnation point of an axially-symmetric body.

The assumption that the entire slab of Teflon is at some uniform temperature during ablation is not realistic. It has been found experimentally that during the ablation process the material is still at the initial temperature a few millimeters below the surface and that a steep temperature gradient exists near the surface. The process is quite complex, and is described by the generalized heat conduction equation as follows:

$$\rho_p C_{p_p} \left(\overline{v} \cdot \Delta T + \frac{\partial T}{\partial t} \right) = Q_p + \nabla \cdot K \nabla T \qquad (1)$$

where Q_p is the heat absorbed per unit volume by the action of depolymerization and $\overline{v}$ is the apparent motion of the Teflon with respect to a coordinate system which is at rest with respect to the ablating surface at the stagnation point.

Equation (1) can be simplified to obtain an approximate qualitative relationship between the ablation rate $\dot{x}$ and the surface temperature of the Teflon, T_w. Over a large portion of any re-entry trajectory, the Teflon appears to be ablating in quasi-steady state, so that $\partial T / \partial t = 0$. In addition, temperature gradients parallel to the surface are small in comparison to those normal to the surface. Since the temperature gradients are largest at the surface, and Q_p is an Arrhenius function of temperature, most of the heat absorption by depolymerization occurs near the surface; hence, Q_p can be assigned to the surface itself. The first order reaction rate then yields:

$$\dot{x} = \int_0^\infty B e^{-E/RT} \, dx \qquad (2)$$

where

$$E = 81,400 \pm 900 \text{ cal/mole}$$

and

$$B = \left(9.4 \; {}^{+7.4}_{-4.2} \right) \times 10^{18} \text{ sec}^{-1}$$

Combination of equations (1) and (2) and integration using constant thermal properties yields the following relation between $\dot{x}$ and T_w:

$$\dot{x}^2 = \frac{\alpha_p B e^{-E/RT_w}}{(E/RT_w)(1 - T_o/T_w)} \tag{3}$$

The plot in Figure 3 would indicate that the surface temperature is relatively insensitive to the ablation rate $\dot{x}$.

This insensitivity makes the Teflon ablation problem simple to approach. A laminar boundary layer analysis (17), in which all species are assumed to have the same physical properties and the pressure gradient is neglected, yields the following expression for the energy transfer in the presence of mass transfer of a combustible gas.

$$-\left(k \frac{\partial T}{\partial x}\right)_{pw} = C_H (\dot{m}) \rho_e u_e \left(H_{e_{air}} - H_{w_{air}} + \Delta H_o C_{o_e}\right) \tag{4}$$

For steady state ablation,

$$-\left(k \frac{\partial T}{\partial x}\right)_{pw} = \dot{m} \Delta H_p \tag{5}$$

Hence

$$\dot{m} / \left[C_H (\dot{m}) \rho_e u_e\right] = \left[H_{e_{air}} - H_{w_{air}} + \Delta H_o C_{o_e}\right] \Delta H_p^{-1} \tag{6}$$

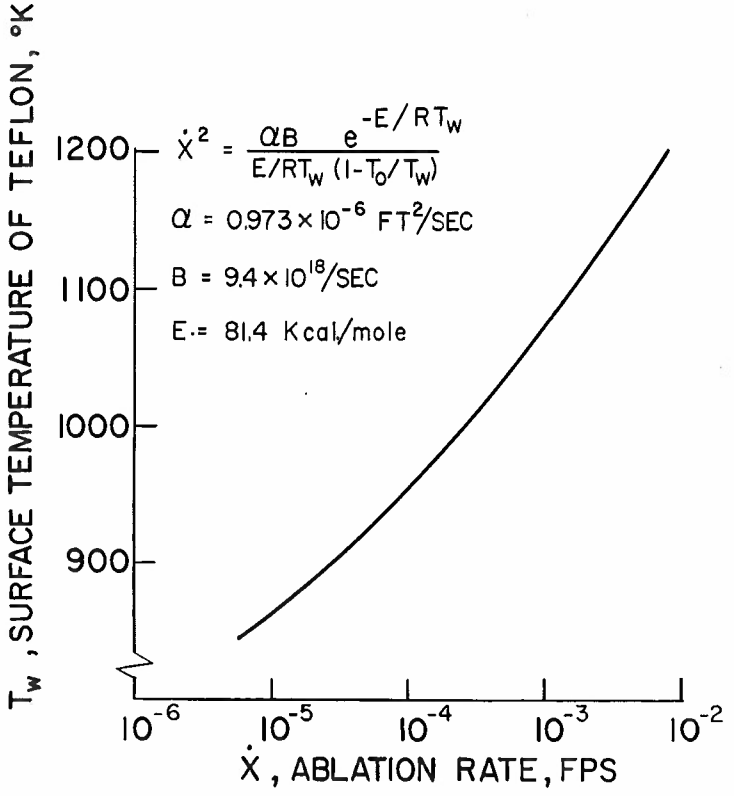

Figure 3. Variation of Surface Temperature With Ablation Rate For Steady State Ablation of Teflon

Since the wall temperature is insensitive to the ablation rate, H_w and ΔH_p may be taken at some average value, and equation (6) yields the ablation rate directly.

For mass transfer into a laminar boundary layer, Stewart (14) has correlated the results of theoretical analyses to obtain the following expression for the Stanton number:

$$C_H(\dot{m}) = C_H(o) - 0.72\,(\dot{m}/\rho_e u_e)\,(Cp_{inj}/Cp_{air})^{0.4} \tag{7}$$

where (Cp_{inj}/Cp_{air}) is effectively $29/M_{c_2 F_4}$. If the heat transfer, given by equations (b) and (7), is equated to the product of the enthalpy increase of the plastic and the steady-state mass transfer rate, the following steady-state value of the heat of ablation can de derived [Sutton (30)]

$$Q^* = \frac{\Delta H_p}{1 + \dfrac{\Delta H_o C_{oe}}{(H_e - H_w)_{air}}} + 0.439\,(H_e - H_w)_{air} \tag{8}$$

It is important to note that for large values of the stagnation enthalpy, $\Delta H_o C_{oe}/(H_e - H_w)_{air}$ is small, hence the effect of combustion may be neglected. Also, for large stagnation enthalpies, the larger contribution to Q^* comes from the second term in equation (8). Hence, doubling ΔH_p will increase Q^* only slightly.

With T_w taken at an average of 1340^oF, $T_o = 100^oF$, $C_{pp} = 0.30$, and $\Delta H_v = 738$ Btu/lb., $\Delta H_p = 1110$ Btu/lb. Using a value of $\Delta H_o = 9380$ Btu/lb., the heat of ablation of Teflon is shown in Figure 4. If combustion is ignored, the theoretical prediction is too large by 20% at the lower enthalpies.

Figure 5 shows the effects of pressure (or altitude) as well as stagnation enthalpy on the ablation characteristics of Teflon. (27). Thus, the heat of ablation for Teflon decreases with increasing stagnation pressure in a manner similar to the Q^* variation of quartz which is discussed in a later section. Experimental results, included in this figure, substantiate the theory with regard to pressure effects. Since combustion effects on the energy transfer to the surface are negligible at the high enthalpy conditions, the theoretical results which neglect combustion are applicable (4):

$$\dot{q} = \dot{q}_{(\dot{m}=o)} - \left(\frac{\Delta\tilde{Q}}{\Delta\dot{m}}\right)_w \dot{m} \tag{9}$$

where

$$\left(\frac{\Delta\tilde{Q}}{\Delta\dot{m}}\right)_w = \frac{15}{m_w}\left[240 \times 10^2 + 1.996 \times 10^{-5} V_\infty^2 - 2.96 \times 10^{-1} T_w\right]$$

To calculate the ablation rate and temperature profiles, the aerodynamic heating rates shown in Figure 2 and the blocking term from equation (9) are used in conjunction with the Goodman integral technique (19) for a semi-infinite slab. (The accuracy of this method is determined by the accuracy of the assumed form of the temperature profile. Figures 6a, 6b, 7, and 8 give typical results.)

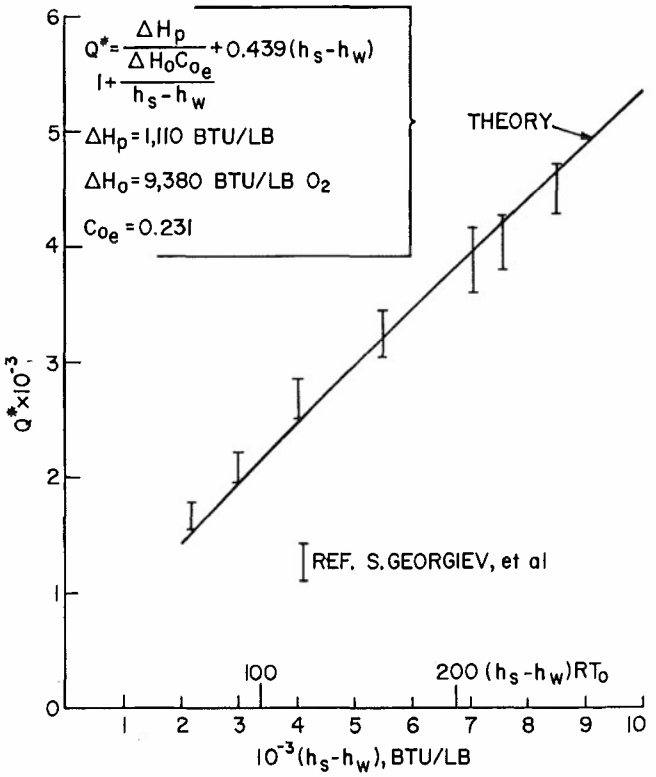

Figure 4. Heat of Ablation of Teflon

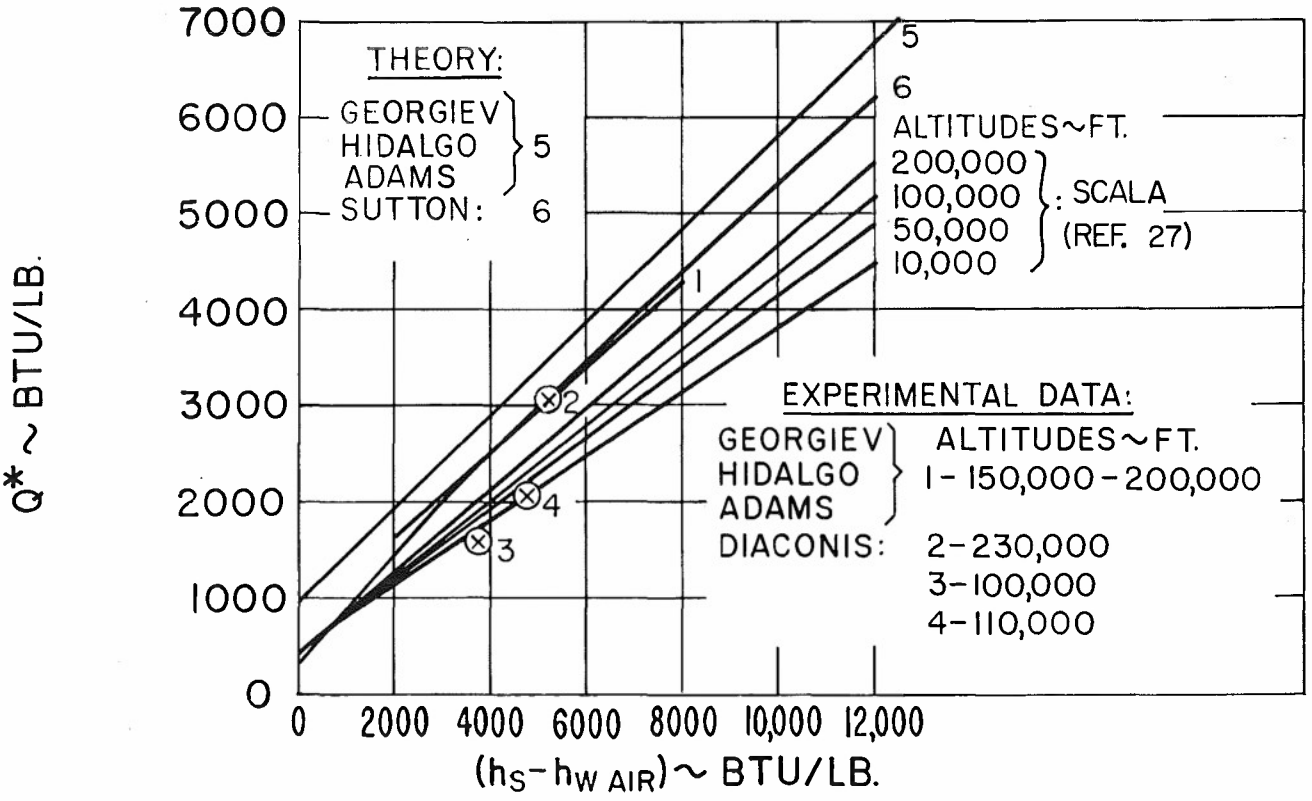

Figure 5. Effect of Altitude on Heat of Ablation of Teflon

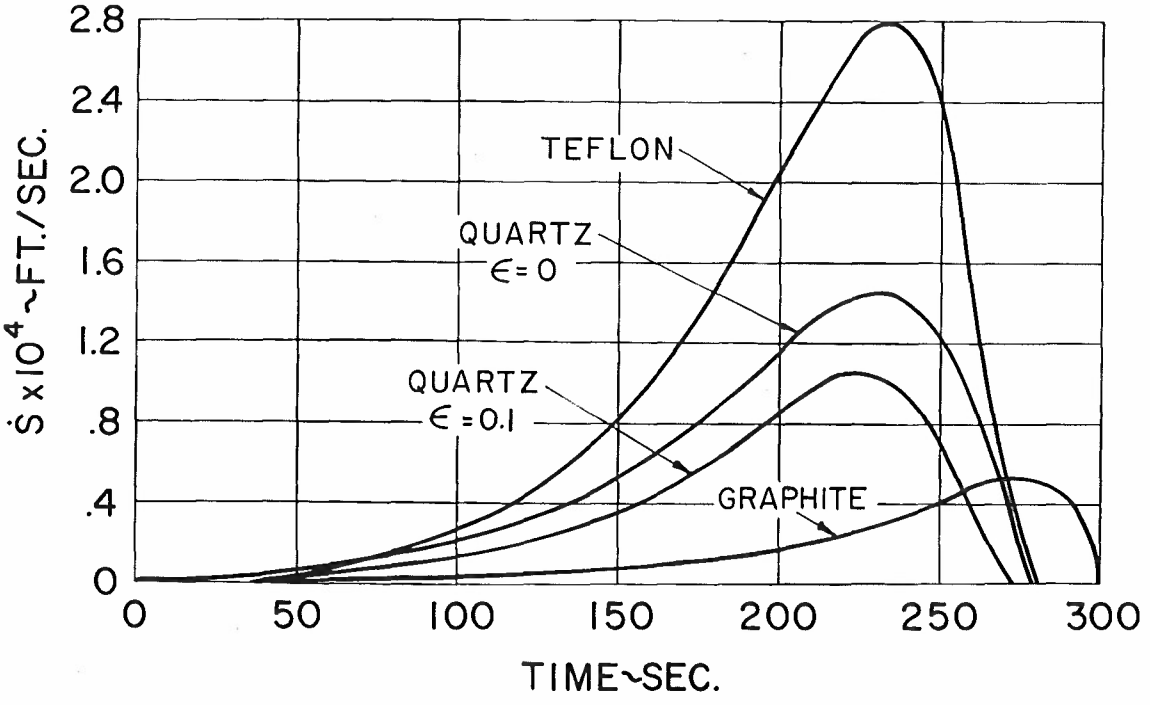

Figure 6a. Ablation Rate for Ballistic Satellite Trajectory
$W/C_DA = 86$

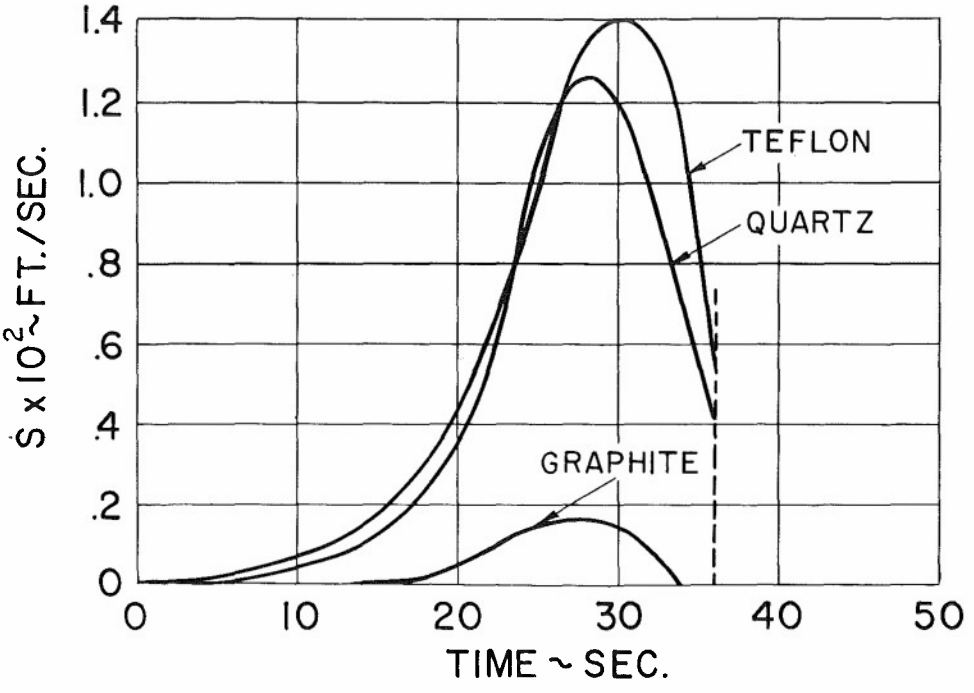

Figure 6b. Ablation Rate for Ballistic Trajectory
$W/C_DA = 2500$

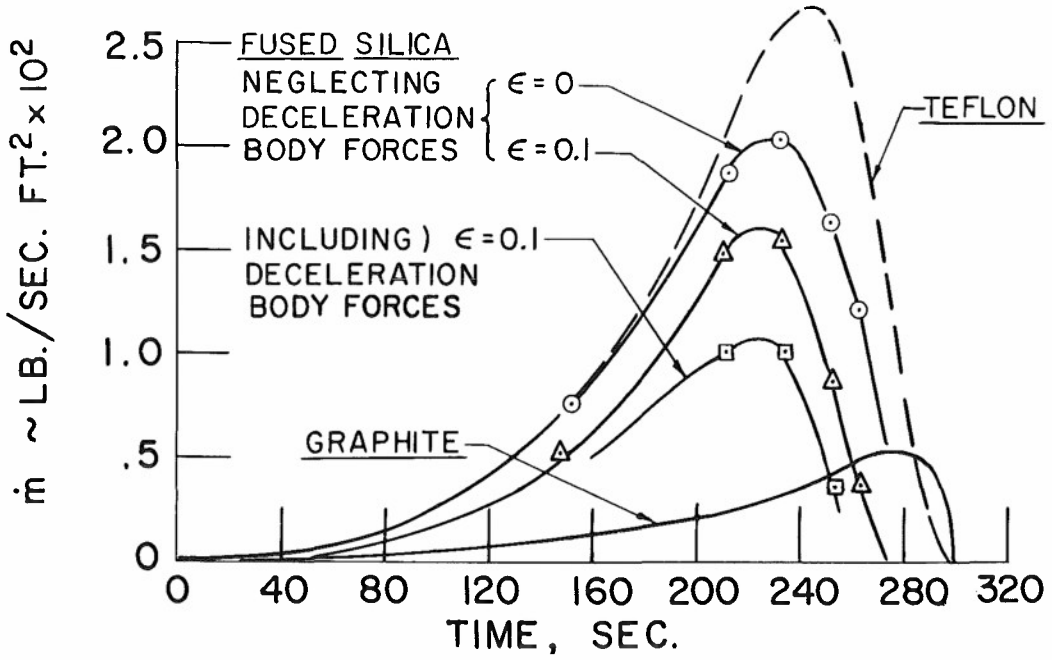

Figure 7. Material Ablation Rates for Re-entry Satellite Trajectory

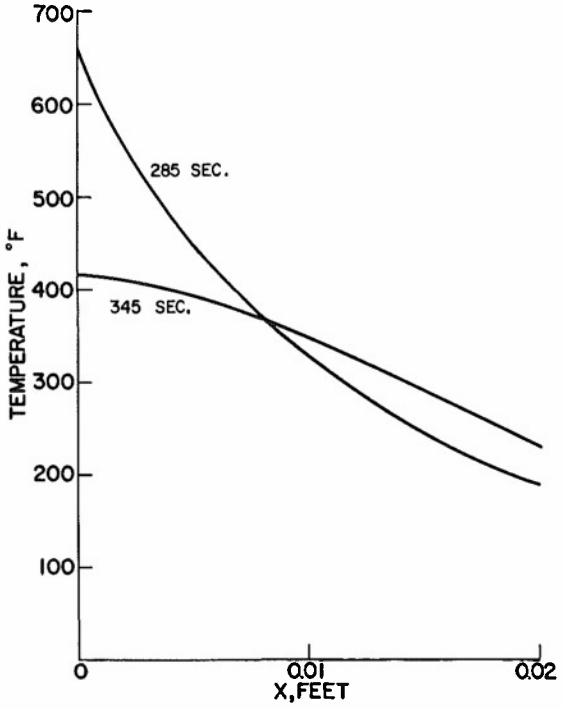

Figure 8. Temperature Profiles in Teflon After Ablation Ends

III. SURFACE COMBUSTION - GRAPHITE

Graphite is typical of the class of materials which undergo surface combustion. The chemical reactions under consideration generally proceed in a sequence of five steps, and include mechanisms for the molecular transport of gaseous reactants to the surface, absorption, combustion and desorption at the surface followed by diffusion and convection of the combustion products into the stream of reacting gas. For re-entry, the combustion reactions involving graphite and dissociated air must be considered. If the surface of the graphite remains at temperatures below $5000^{\circ}R$ (the usual situation), it may be anticipated that the nitrogen atoms present in dissociated air will have recombined in the gas phase. Since nitrogen molecules are chemically inert in the presence of carbon, only oxidation reactions need be considered.

Both carbon dioxide and monoxide have been found experimentally to be present. Therefore, two oxidation reactions may be assumed for the determination of the graphite ablation rate. The first process consists of the formation of both CO and CO_2 in a reaction between C and O_2 at the surface. The second reaction entails the formation of CO_2 in a reaction between C and O_2, followed by reactions with the gas phase to form CO.

A simple model was employed for the analysis of the reactions between the multi-component C-O-N system because of the lack of reaction rate data. In addition, simplifying assumptions of the conservation equations for the gas phase have been made (27). The gas phase has been represented by a three-component frozen mixture of nitrogen, atomic oxygen and carbon monoxide. The surface combustion product is assumed to be carbon monoxide, and nitrogen reactions were not considered at the surface. Finally, the Lewis number was assumed constant and equal to 1.2, while the Prandtl number was taken to be 0.75. With the above assumptions, the ablation rate of graphite at the stagnation point of a blunt body of revolution is given by the following simple relation:

$$\dot{m}_w \cong 0.1 \sqrt{(2 \rho_{gw} \mu_{gw} \beta)} \tag{10}$$

Equation (10) applies in the diffusion-controlled ablation regime where the ablation rate is insensitive to surface temperature, provided that the surface temperature exceeds 1000° R.

Assuming a Newtonian pressure distribution over the body, equation (10) may be further simplified to the form:

$$\dot{m}_w \sqrt{R_B} = 5 \times 10^{-6} \sqrt[4]{\frac{P_e^3}{\rho_e}} \tag{11}$$

Substitution of typical re-entry pressures and densities into equation (11) yields the values of $\dot{m}_w$ shown in Figure 7. These lead to the conclusion that in the case of satellite re-entry, graphite has such low thermal erosion characteristics that it may be considered primarily as a heat sink material which undergoes oxidation reactions with the environment.

Considering heat transfer into the interior of the graphite, an energy balance reveals that:

$$-k \left(\frac{\partial T}{\partial x} \right)_{sw} \quad \dot{q}_{aero} - \left[\left(\frac{\Delta \tilde{Q}}{\Delta \dot{m}} \right)_w + h_{gw} - h_w(s) \quad \dot{m}_w \right] \tag{12}$$

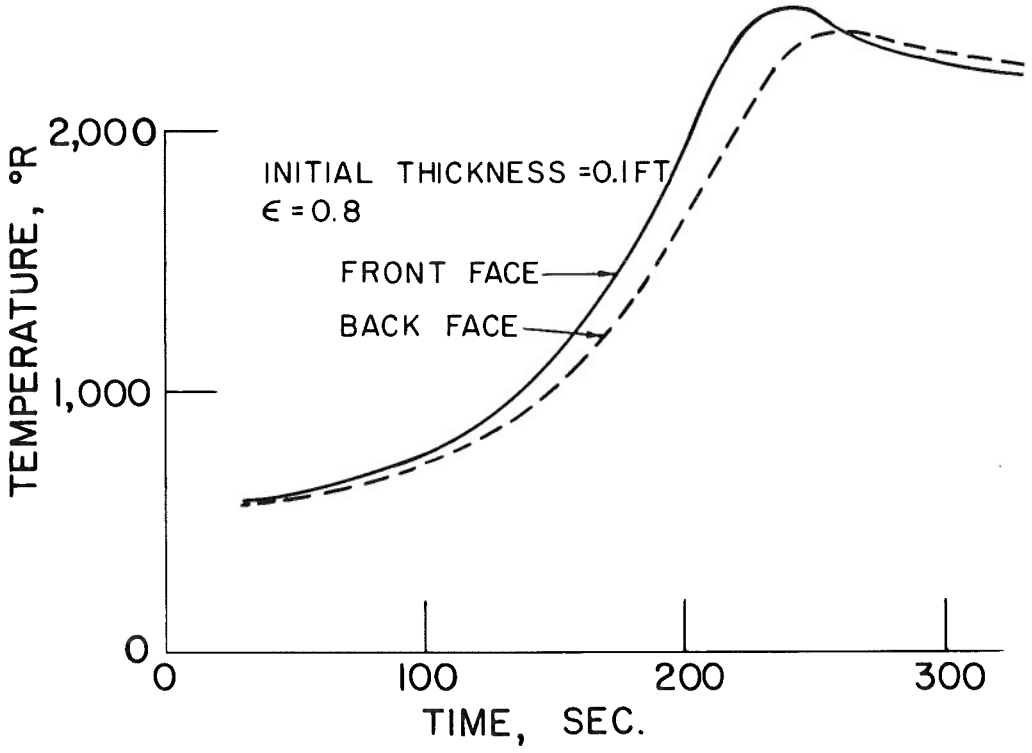

Figure 9. Front and Back Wall Temperatures of Graphite for Re-entry Satellite

The ablation rate $\dot{m}_w$ of the graphite due to surface combustion is extremely small for the low stagnation pressure re-entry trajectories (satellite re-entry). Consequently, the heat transfer to the surface would be altered primarily due to the large negative heats of formation of the combustion products. This is reflected in the term h_{gw} which may be a negative quantity. At low wall temperatures, the chemical heat release actually exceeds the blocking action due to injection of the products of combustion into the gas phase. It is possible, under these conditions, for the term $-(k\,\partial T/\partial x)s_w$ to be larger by 20 per cent than the aerodynamic energy transfer to the surface.

Recent theoretical and experimental results for the ablation of graphite at laminar stagnation point in dissociated air (50, 27) are given in Figure 32.

Thus, the design of a thermal shield utilizing graphite is limited not by its ablation rate, but rather by the heat penetration aspects and, consequently, mechanical limitations such as thermal shock and shield fastening problems. The front and back wall temperatures of a layer of graphite 0.10 inches thick, with a surface emissivity of 0.8, are shown in Figure 9, for the case of variable thermal conductivity.

IV. MELTING AND VAPORIZATION - GLASSES

There are few practical materials which sublime directly, or which have sufficiently high vapor pressures at their melting point to give flash vaporization. To obtain appreciable vaporization, with its associated heat absorption and boundary layer thickening, materials are required whose melt is highly viscous, so that the liquid can be heated to near-boiling temperatures before aerodynamic forces remove it. Such materials are by their very nature glasses; e.g., liquids which are sufficiently viscous that they may be super-cooled without the molecules falling into the ordered array of a crystal. Data on glasses indicate that fused silica has the highest viscosity and under certain conditions this material has given evidence of superior ablation characteristics (7, 11).

In addition, high silica content glasses are quite resistant to thermal shock. They are, however, transparent to infrared radiation and consequently often have additives dispersed throughout to absorb or scatter both incoming radiation and self radiation from the heated surface.

When vaporized, silica forms both the gaseous dioxide and monoxide, in the following highly endothermic reactions:

$$SiO_2(s) \rightleftharpoons SiO_2(l) \rightleftharpoons SiO(g) + \frac{1}{2} O_2(g) \tag{13}$$

$$SiO_2(s) \rightleftharpoons SiO_2(l) \rightleftharpoons SiO_2(l)$$

Thus, the heated solid dioxide softens and forms a liquid layer which vaporizes and injects the gaseous dioxide, the monoxide, and the oxygen into the gaseous boundary layer. Thus, glasses absorb heat in several ways. The melt flows downstream and blocks a portion of the heat from the solid, the vaporized species thicken the gaseous boundary layer and consequently decrease the heat flux to the surface, and finally there is heat absorption by phase changes. In addition, the high surface temperature can re-radiate an appreciable fraction of the heat flux.

To determine the effective heat ablation, Q*, the characteristics of the flow of a liquid layer under the influence of a hypersonic gaseous boundary layer with mass transfer have been determined. The equations describing the liquid are highly complex due both to the variation of viscosity with temperature and to the required matching at the interface with a dissociated gaseous hypersonic boundary layer.

An analysis has been made by Fanucci and Lew (22) for the flow of a liquid layer with vaporization under the influence of a gaseous hypersonic boundary layer (laminar or turbulent, depending on the region of the body concerned), with proper account of the history of the flow from the stagnation point. Some results of the characteristics of the liquid phase at the stagnation point of the satellite vehicle have been matched with an analysis of Scala (23) for the dissociated hypersonic boundary layer with mass addition to obtain the rate of ablation of the surface, the fraction vaporized, $\Gamma$and the effective heat of ablation, Q*.

The heats of ablation for steady-state conditions are shown in Figure 10. An increase in stagnation pressure causes the surface temperature to rise, resulting in a decrease of the viscosity of the liquid layer and a decrease in Q*. The lessened viscosity causes more material to flow downstream under the influence of aerodynamic forces, resulting in a smaller gasification ratio. On the other hand, Q* increases in a nearly linear fashion with increasing stagnation enthalpy, because the higher heat transfer rates at high stagnation enthalpies force more of the liquid to vaporize.

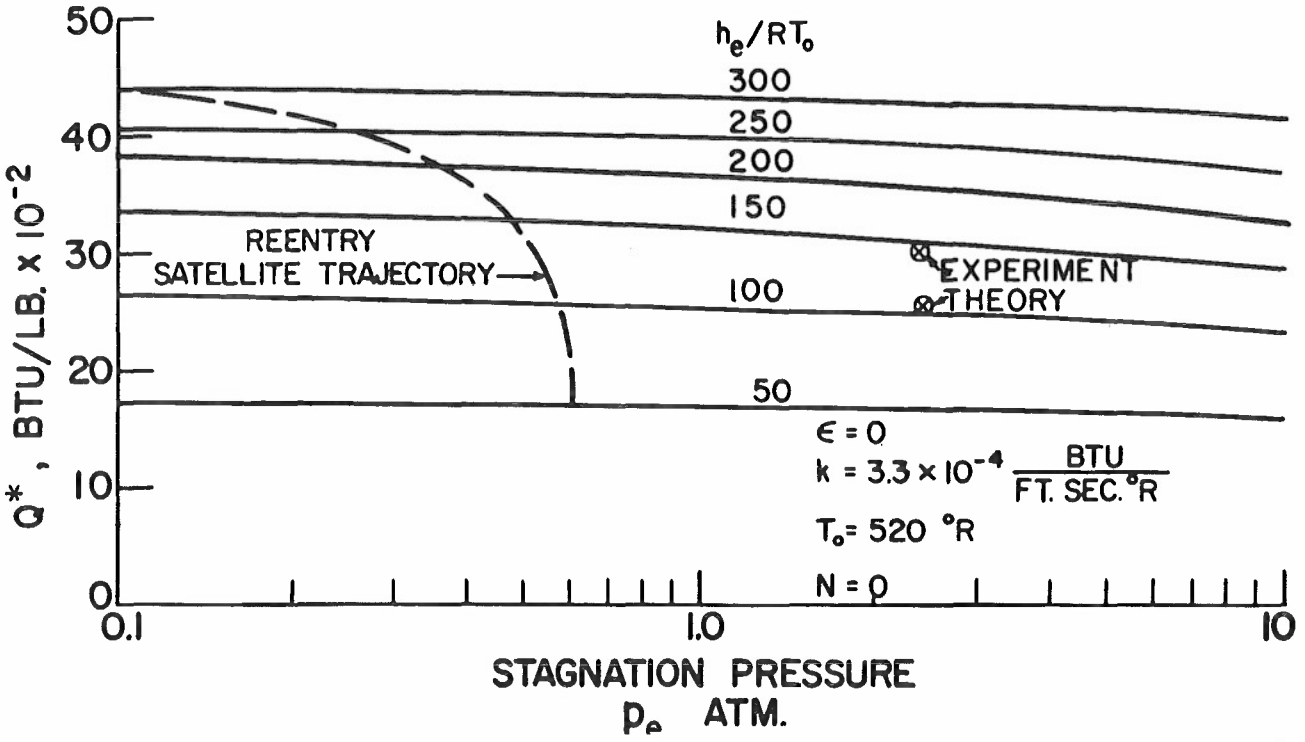

Figure 10. Variation of Q* With Stagnation Pressure and Stagnation Enthalpy for Fused Silica

The variation of Q* along the trajectory of the re-entry satellite is indicated in Figure 10. The associated surface temperatures are shown in Figure 11; there is little surface temperature variation for steady flight at each altitude and velocity of the re-entry satellite trajectory. It is clear that during the actual trajectory the initial temperature of the silica is low, and no ablation will occur until the silica is heated above its softening point. This occurs at about 160 seconds when the ablation process begins.

A study of the effects of deceleration, and hence of body forces, indicates that Q* is increased, and the net mass loss over a trajectory is decreased. This effect is shown in Figure 7 and is not negligible even though the rate of deceleration is low. Another factor considered was the effect of surface re-radiation on Q*. Clearly, surface re-radiation will decrease the net heat transfer to the surface. In Figure 7, it also may be seen that a very modest emissivity of 0.1 decreases the ablation rate by about 20%. If the surface emissivity is unity, then the equilibrium temperatures will be 3470° R for the case of no heat conduction into the interior. Under these conditions, the silica probably will not ablate but will act merely as a re-radiating surface. If the thickness is sufficiently large, then the silica will act as a heat sink, with a maximum surface temperature of 2800°F. A heat sink calculation yields a maximum value of the net heat transfer of 28 Btu/ft^2-sec and a heat pulse of about 5000 Btu/ft^2. The thickness of silica required to yield a final back-face temperature rise of 200°F is about 7 inches, and is inversely proportional to the final back-face temperature rise; a thickness of one inch will yield a back-face temperature rise of 1400°F. On this basis, it appears more desirable to have the emissivity of the silica less than unity so that a surface temperature sufficiently high to cause ablation is reached, resulting in a decrease of the net heat content of the remaining silica. Thus quartz, when utilized as a heat sink, is relatively inefficient.

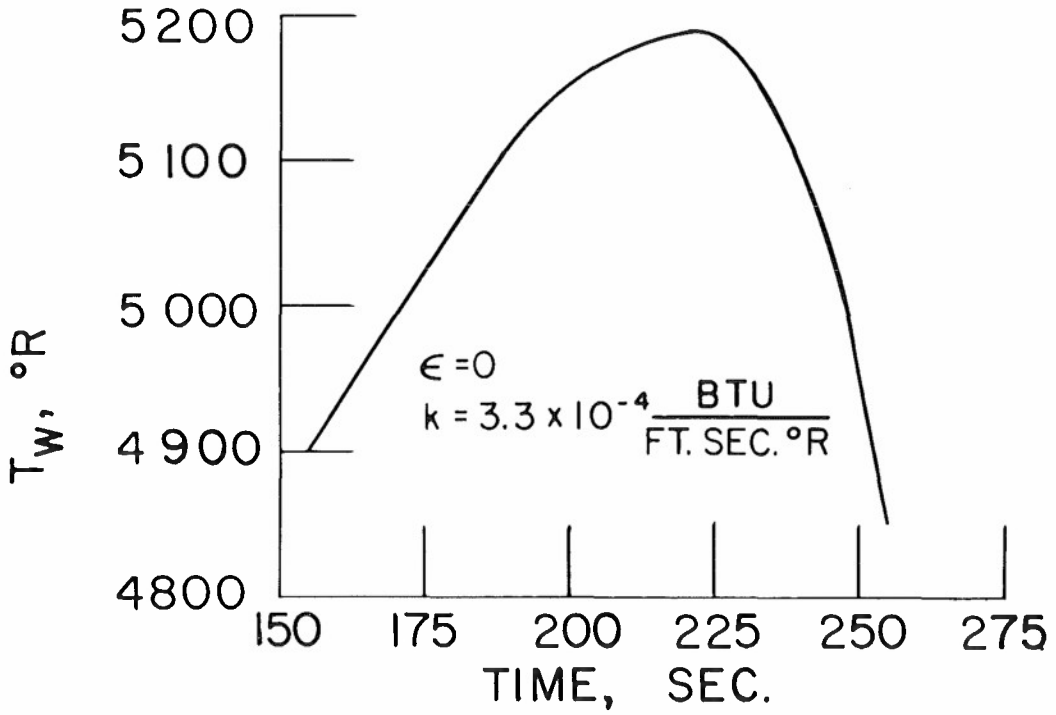

Figure 11. Surface Temperature History for Fused Silica

Non-equilibrium vaporization effects have been considered by Scala and Vidale (24, 25). It was found that rate controlled vaporization tends to increase the surface temperature resulting in a decrease of Γ and Q^* above 200, 000 ft. The effect is not significant since ablation will probably not begin at altitudes above 200, 000 ft. for satellite re-entry.

Time-dependent environmental conditions on melting and vaporizing ablation (glassy material) of blunt-nosed bodies have been recently considered by Chen, et al. (37), who consider a time-dependent flow past a stationary semi-infinite body. Chen concludes that transient effects should not be neglected. It should be noted that the effects of deceleration forces corresponding to flight have been determined theoretically for the stagnation point. Preliminary results indicate that the effects of deceleration forces (quasi-steady state) are only important for the stagnation pressure levels of satellite re-entry (cf. Figure 7).

The comparatively simple behavior (relative to charring materials) and generally good ablation characteristics of this class of materials have resulted in extensive treatment (8, 9, 10, 40, 41, 34, 53).

V. REINFORCED PLASTICS

Reinforced plastics include some of the most attractive materials for use in satellite re-entry. Certain of the phenolic, silicone and melamine resins make suitable resins (7); 91LD resin (Cincinnati Testing Laboratories), for example, has shown good characteristics experimentally. When heated, this resin pyrolyzes into a gas and a carbonaceous structure which shrinks in dimension. Preliminary experiments indicate that the gas is composed of hydrogen, methane, and carbon dioxide. Combustion may occur between methane and oxygen to form CO_2, H_2O, OH and CO. The latter three then may react with and chemically erode the carbonaceous structure to form CO and CO_2. Suitable reinforcements include "E" glass, Refrasil (a form of silica: H. T. Thompson Co.), and nylon (7, 11).

Phenomenological behavior in this class varies significantly with time and magnitude of heating. For the application under consideration, the nylon-reinforced plastic pyrolyzes to form a moderately thick, low density, charred layer which in general has shrunk dimensionally and which may have been chemically eroded at the surface. The surface temperature of the char layer may become sufficiently hot to re-radiate most of the aerodynamic heat. The heat damage propagated into the material thus is caused by the aerodynamic heat transfer and by the heat released during combustion or chemical reaction within the char and adjacent layer.

For glass and refrasil reinforcement, char depth was found experimentally to be about twice that of the nylon reinforcement. When inorganic fibers are used as reinforcement, the plastic tends to delaminate and grow in dimension (13). The local rate at which unpyrolyzed plastic is pyrolyzed depends to a large extent on the kinetics involved.

The problem of predicting the rate of pyrolysis of the plastic is thus quite complex. Steady state ablation does not appear probable for re-entry satellites protected by reinforced plastics. Redefining therefore Q^* by $Q^* = Q_{(\dot{m}=0)}/m_p$ where $\dot{m}_p$ is the rate at which mass is pyrolyzed but not necessarily removed, Scala has obtained the following expression:

$$Q^* = (\Gamma + \Xi) \left[\left(\frac{\Delta Q}{\Delta m} \right)_w + H_{gw} \right] - H_{vp} \tag{14}$$

To evaluate Q^*, the chemistry of the interaction between the material and dissociated air must be considered.

If pyrolysis occurs in a vacuum, then $\Gamma \dot{m}_p$ represents the rate of gasification, and $1 + (1 - \Gamma)\, \dot{m}_p$ represents the rate of formation of char, where $\dot{m}_p$ is the rate of pyrolysis. During hypersonic re-entry, however, oxygen diffuses toward the surface and oxidation reactions occur.

With this combustion, the rate of gasification is given by $(\Gamma + \Xi)\dot{m}_p$, and the instantaneous rate of char formation is $(1 - \Gamma - \Xi)\dot{m}_p$. It is clear that the char is continuously formed at an interface between the virgin plastic and the pyrolyzed layer, and, if sufficient oxygen diffuses to the surface, is consumed at the outer surface. Thus, the rate of growth of the char layer depends on:

a. the mass diffusion flux of oxygen from the main stream toward the surface, and
b. the quantity and reactivity of the combustible gases produced during pyrolysis which flow into the boundary layer; this, in turn, is controlled by the rate at which heat can be conducted to the virgin plastic.

The ablation of phenolic nylon is considered now in greater detail. An exact solution for air injection into the hypersonic dissociated stagnation point laminar boundary layer yields the following expression for the heat blocked due to mass transfer (23).

$$\frac{(\Delta Q)}{\Delta \dot{m}_w} = \frac{30}{M_w} \left[240 + 0.48 (H_e - H_w) \right] \tag{15}$$

This is assumed to be valid for predicting the effects of gas injection containing species other than oxygen and nitrogen. Since the mean molecular weight of the gas at the surface appears in the denominator, the injection of light-weight gases such as hydrogen enhances the blocking term.

If nylon is utilized as a resin, it melts, vaporizes and reacts without leaving a char residue (11), while phenolic resin decomposes to form a char residue. Nylon and phenolic resin combined in equal amounts by weight may be represented by the empirical formula $C_{13}H_{18}O_2N$. The behavior of the composite material is such that:

a. light-weight gases are released during pyrolysis.

b. a char layer is formed which enhances re-radiation from the surface.

A theoretical analysis of the ablation of phenolic nylon, utilizing the boundary layer equations, is complicated by the large number of different chemical species which are the original products of pyrolysis and by the subsequent combustion reactions between these species and the components of dissociated air. Experimental data (11) indicate that under vacuum conditions $\Gamma \approx 0.7$. Hence, $0.7 < (\Gamma + \Xi) \leq 1$.

The dependence of the heat blocking action term $(\Delta Q/\Delta \dot{m})_w$ on the mean molecular weight, M_w, has been noted above. If, for example, the final products of gaseous dissociation and combustion are primarily hydrogen, with small amounts of water and carbon monoxide, the heat blocking term can easily be a factor of two or three larger than the corresponding term for transpiration cooling by air injection. Another effect contributing to Q^* is the magnitude of the gaseous enthalpy at the surface, H_w. Combining equations (17) and (18) indicates that Q^* tends to increase approximately as the additive term $(1/2)\, H_w$. The more hydrogen at the surface, the larger the term H_w will be.

Finally, it is observed that complex hydrocarbons such as phenolic-nylon have a negligible heat of formation per unit mass, and therefore H_{vp} is essentially zero.

On re-examination of equation (17), in the light of the foregoing discussion, Scala has estimated that Q^* may be approximated by:

$$Q^* = 1500 + \frac{1}{2} H_e \tag{16}$$

A detailed theoretical description leading to the prediction of the thermal response of a char-forming plastic presents major difficulties, rooted in structural-physicochemical-aerodynamic interactions. A number of models have been proposed. Barriault and Yos (43) consider a steady state model of a porous outer layer through which the gases of plastic decomposition flow, backed by a semi-infinite layer of undecomposed plastic. The porous layer corresponds to the charred layer and it is assumed that the gas flow flows freely through the char.

The induction time of the non-steady phase of ablation is also derived. This formulation has not as yet yielded numerical results. Gilbert and Scala (38) have considered the thermal response of a typical phenolic-type resin and the structural behavior of the resulting char. This analysis leads to a prediction of the spallation behavior of the char provided the failure stresses and mode of failure are known.

Composite plastic materials reinforced with glassy fiber have been considered from an aerodynamic point of view by Georgiev, et al. (42). The method analyzes the liquid layer by a theory applicable to glass behavior. The plastic component is assumed to vaporize completely as in Teflon, for example. The heat of ablation is the sum (weighted by mass fraction) of the heat of ablation of the glass component and the plastic component. A continuous liquid layer is assumed to exist, requiring a glass mass fraction in excess of 50%, according to the authors.

Some thermo-chemical aspects of glass-reinforced plastic ablation have been considered by Beecher and Rosensweig (39), who take into account the thermal decomposition of the resin and the chemical reactions between the gaseous products and between carbon and fiberglass. They find that the last reaction acts as a heat sink, which affords a possible theoretical basis for the heat of vaporization assumed by Adams (42) in his model of fiberglass material behavior.

VI. EXPERIMENTAL RESULTS

6.1. Experimental Facilities and Procedure

The experimental data described below were obtained in electric arc heated facilities (28 and 33). Their characteristics are given in Table I. The simulation of free flight stagnation conditions are summarized in Figure 12; it is seen from this figure and Figure 1 (cross-hatched area) that a large portion of the re-entry profile is covered.

TABLE I

CHARACTERISTICS OF AIR ARC TEST FACILITIES

	Shroud Arc	Supersonic Arc Tunnel
Stagnation Enthalpy h_s, Btu/lb.	3400-6800	1300-7400
Stagnation Pressure $P_{s,pl}$, psia (1), (2) correspond to test arrangement below	1. 30-75 2. 15-23	4.3 - 14.7
Heating Rate (Btu/ft.^{2} sec.)	300 - 3000	3 - 100
Testing Time	~ 30 secs.	$\geq$ 1000 secs.
Contamination of Heated Air (by weight)	< 4% carbon	< 4% carbon
Existing Test Arrangements	1. Model shrouded by shaped nozzle, $P_{s,pl} = P_s$ 2. Model in free subsonic jet, $P_{s,pl} = P_s$	Wind Tunnel Mach 5 flow $P_{st} < P_{s,pl}$
Nominal Model Dimension, Range	1. 1.5" d. 2. 0.75"d.	1.5"d.

$P_{s,pl}$ = plenum (stag) pressure

P_s = model stagnation region pressure

Figures 13 a, b show an arc tunnel facility and a view of the test flow. A continuous low heating rate environment in flows of high stagnation enthalpy levels and high supersonic Mach numbers is available. A relatively simple device, it uses a continuous electric arc to heat the test gas; the gas is then expanded through a supersonic nozzle to the test section. Stagnation test properties are controlled by the throat of the supersonic nozzle, heat transfer rates are available up to 100 Btu/ft.^{2} sec. for test periods greater than five minutes duration.

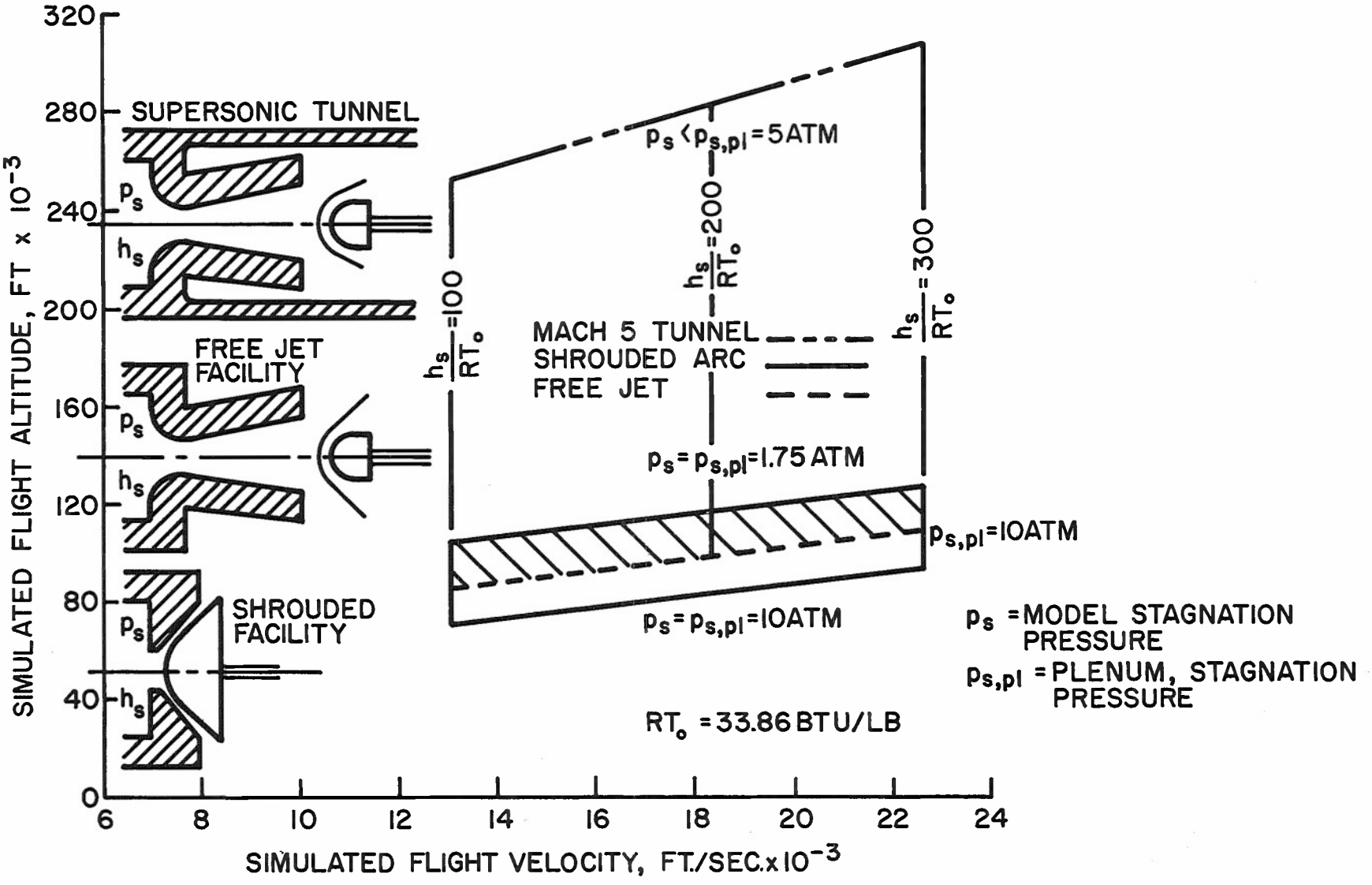

Figure 12. Air Arc Simulation of Free Flight Stagnation Conditions

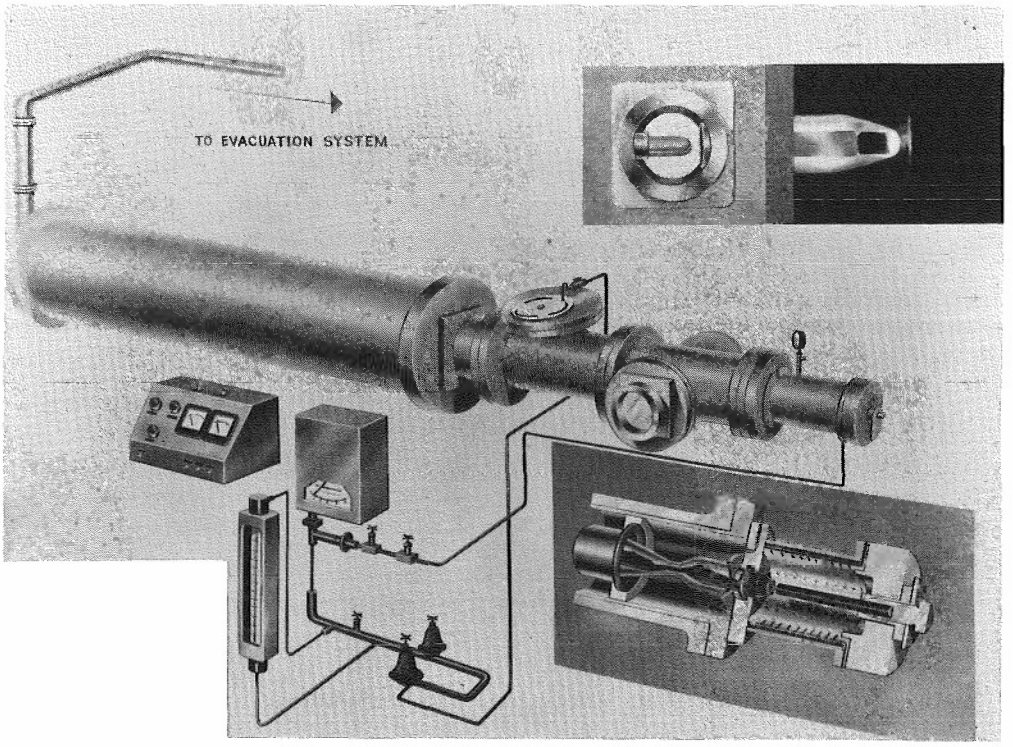

Figure 13a. Electric Arc Heated Supersonic Wind Tunnel

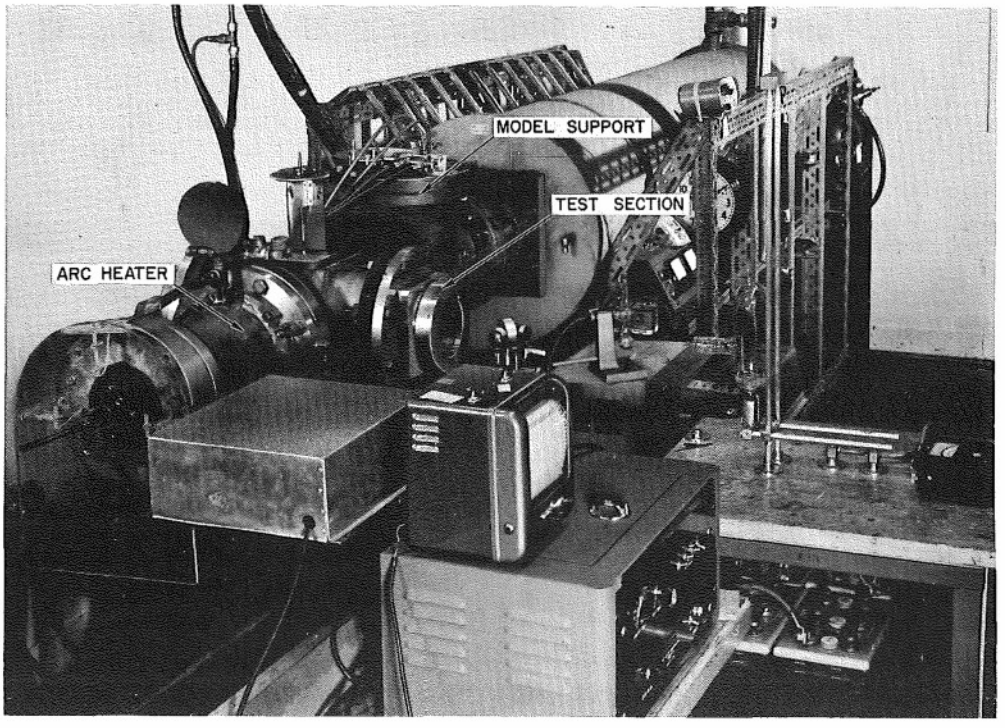

Figure 13b. Supersonic Arc Wind Tunnel

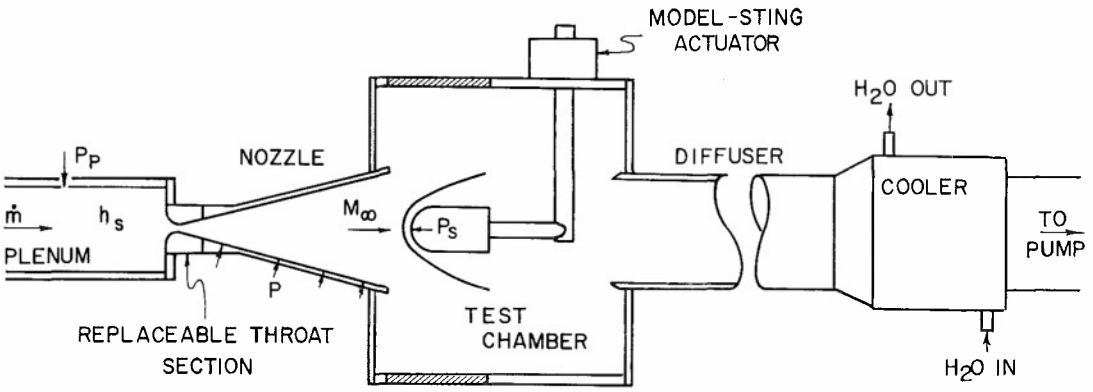

TYPICAL TEST MEASUREMENTS

MODEL	FACILITY AND CALIBRATION
1. SURFACE T	1. VOLTAGE AND CURRENT
2. SUB-SURFACE AND BACKWALL T	2. ELECTRODE EROSION RATE (IF APPROPRIATE)
3. SURFACE P	3. AIR MASS FLOW RATE
4. SURFACE $\dot{q}_o$	4. P_P
5. ABLATION RATE-LOCAL AND TOTAL	5. GAS T-THROAT, PLENUM, TEST SECTION
6. FORCES - 3 COMPONENT	6. h_S CALORIMETER-TEST GAS
7. FLOW PHOTOGRAPHY	7. NOZZLE STATIC PRESSURE - P
	8. $\dot{q}_o$ PROFILES - TEST SECTION
	9. P_S PROFILES - TEST SECTION
	10. LUMINOSITY - FLUCTUATIONS - TEST GAS

Figure 13c. Characteristics of Supersonic Arc Wind Tunnel

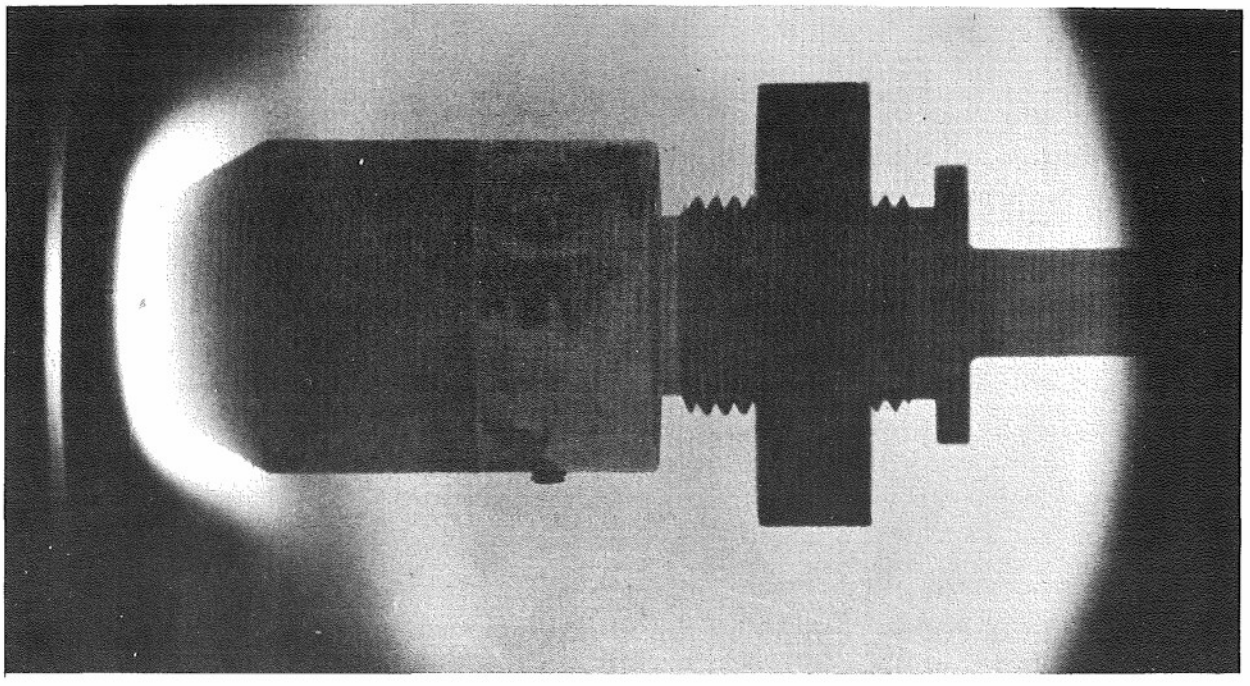

Figure 13d. Stagnation Point Model in Test Flow 1-1/2 Inch Diameter Model

The insert in Figure 13-a shows a sectional view of the arc chamber, electrodes, plenum chamber, primary throat, and conical nozzle. During operation, air is injected tangentially into the arc chamber. An arc is struck between the two electrodes, and the gas passes through the annular electrode into the plenum chamber, expands through the nozzle to the test section, and then exhausts through a vacuum system. In this unit, all sections except the electrodes are consumed at a slow rate during operation; much of the electrode material is deposited along the walls of the plenum chamber but some remains in the heated air, resulting in some contamination (see Table 1).

Operating conditions of the arc tunnel can be varied over appreciable ranges of flow parameters. Most of the tests reported herein were performed at nominal flow properties of $P_{s,pl} = 270$ mm Hg absolute, $M_t = 4.80$, $P_{st} = 5.5$ mm Hg absolute, and $h_s = 5900$ BTU/lb.

The shroud nozzle technique (Figure 14) involves the production of a desired pressure distribution over a test surface by properly contouring the nozzle walls. This concept (due to Ferri and Libby, Ref. 29), combined with an electric arc heater to permit the testing of relatively large models with a minimum of electric power, produces a subsonic flow field about hemispherical models with equivalent facility and model stagnation properties. It is a high heat transfer rate facility; heat transfer rates of 300 - 3000 Btu/ft.^{2} sec. are available.

The shroud nozzle contours are chosen to correspond to a streamline for an incompressible potential flow over a sphere at the stagnation conditions of gas stream, which leads to pressure distributions particularly useful in the study of stagnation point ablation. As the model ablates during the test, constant properties are maintained in the shroud by establishing choked flow between the model and nozzle by a constant model feed. Examination of the model surface curvature at the stagnation point after the test indicates that geometrical changes are insignificant; surface pressure measurements near the stagnation point agree with the predicted potential flows within a small percentage scatter.

Measured stagnation-point non-ablating (calorimeter) heat-transfer rates and pressure gradients agree with predicted heat transfer and enthalpies (26) to within 10% for both facilities. Spectroscopic measurements of the test gas temperature without a model present in the flow check the experimentally determined enthalpy level to the same accuracy.

The effect of electrode contamination of the arc stream is important since it would be desirable for accurate simulation to have the concentration of free oxygen in the arc stream the same as that in air. Depletion of oxygen can affect the performance of those ablation materials where combustion can occur. Materials, such as quartz, however, are not affected to any extent.

The contamination of the arc stream by carbon electrodes or by copper electrodes has been studied in detail by Wachman and Linevsky (44, 45, 46). When carbon contaminates the air stream, carbon monoxide is formed diminishing the quantity of free oxygen. These results are illustrated by Figure 15, where the decrease in relative atomic oxygen concentration and the increase of relative carbon monoxide concentration are shown for various percentages of carbon in the mixture. (relative concentration is a ratio of mole fraction of gas in a given air-carbon mixture to the mole fraction of the gas in air.) The enthalpy function of the air carbon mixtures has a minimum at about 15% carbon contamination (cf. Figure 16). Cooled metallic electrodes,

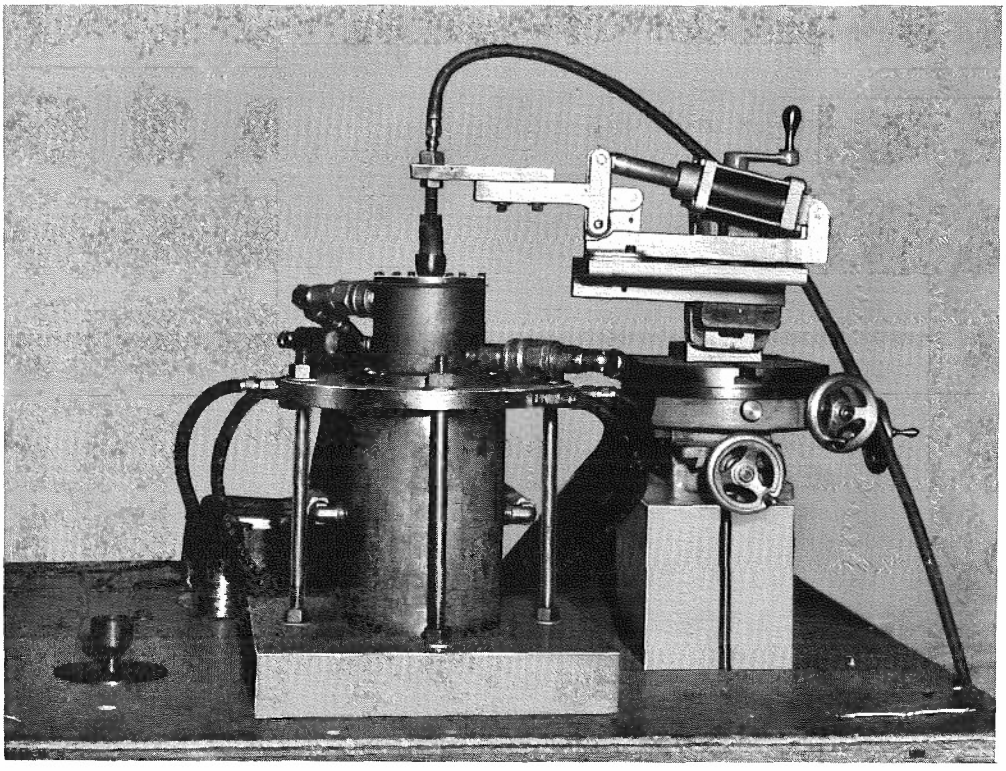

Figure 14a. Photo of Shrouded Arc

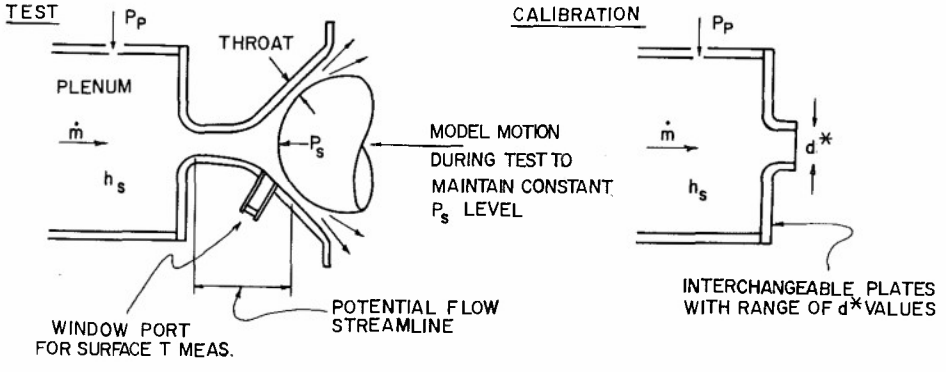

TYPICAL TEST MEASUREMENTS

MODEL	FACILTY AND CALIBRATION
1. SURFACE TEMPERATURE	1. VOLTAGE
2. SUB-SURFACE AND BACKWALL TEMPERATURE	2. CURRENT
3. SURFACE PRESSURE	3. ELECTRODE EROSION RATE (IF APPROPRIATE)
4. SURFACE HEAT TRANSFER RATES-NON-ABLATING	4. AIR MASS FLOW RATE
5. ABLATION RATE-LOCAL AND TOTAL	5. PLENUM PRESSURE
	6. GAS TEMPERATURE - THROAT
	7. GAS TEMPERATURE - PLENUM

Figure 14b. Characteristics of Shroud Arc Test Facility

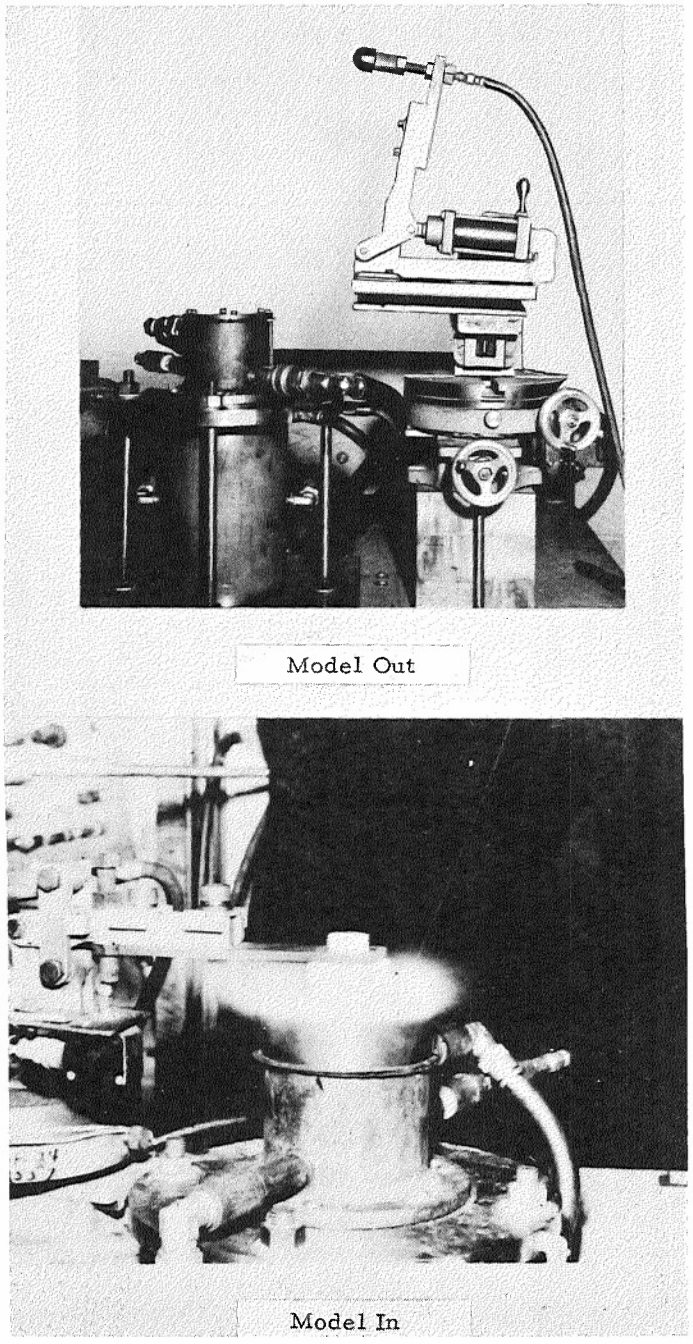

Figure 14c. Ablation Test in Shroud Arc Facility

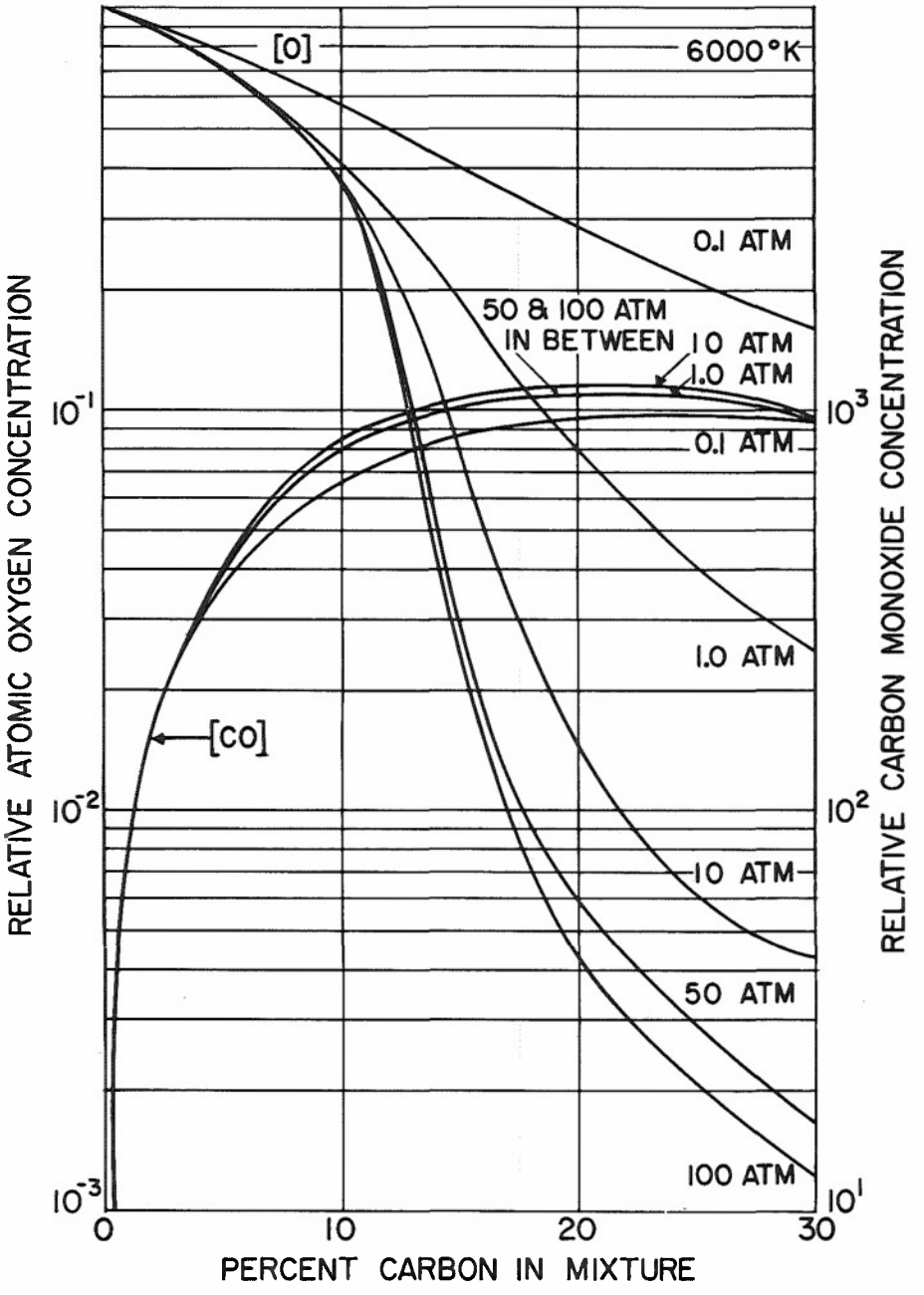

Figure 15.

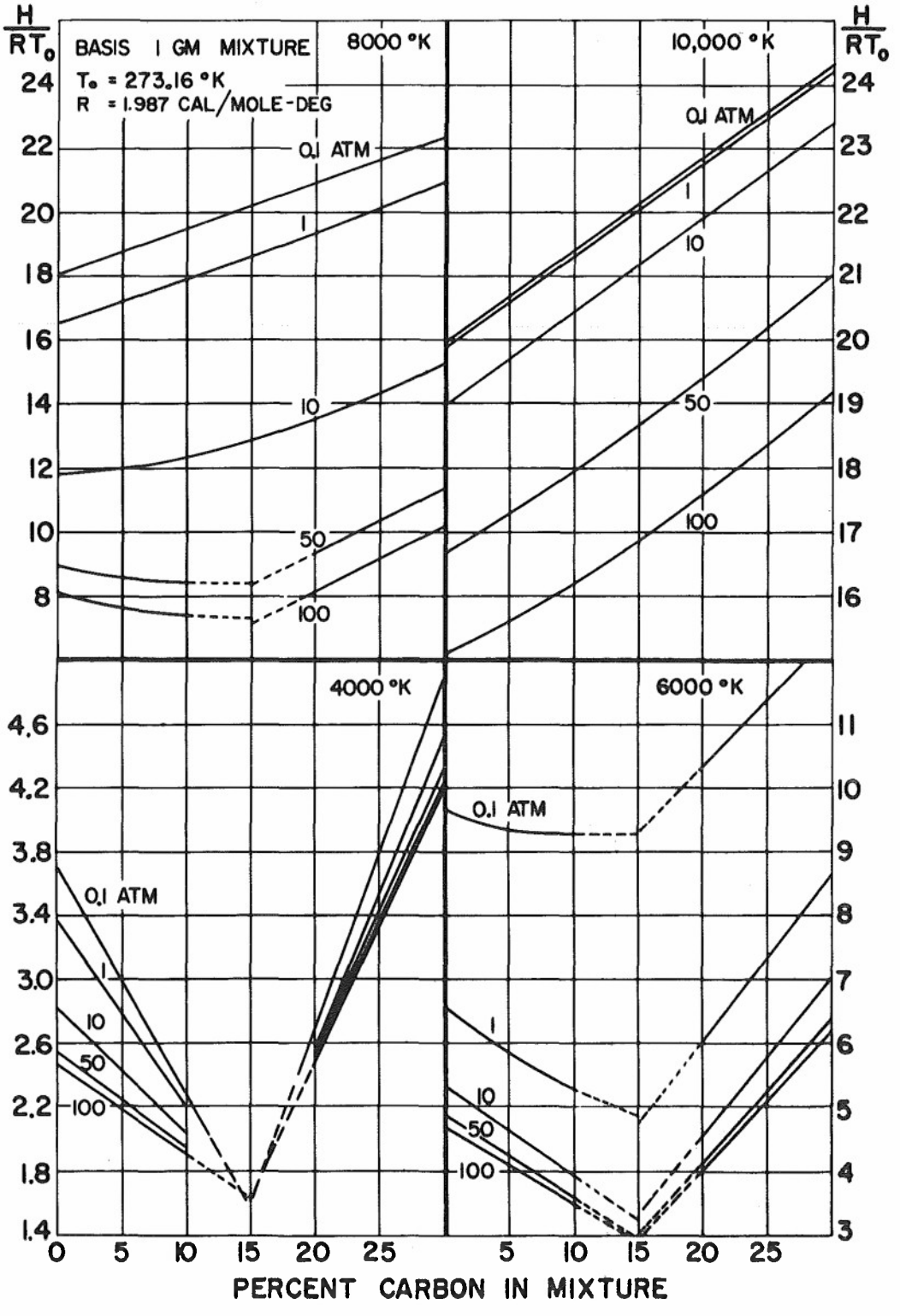
H/RT₀
BASIS 1 GM MIXTURE
T₀ = 273.16 °K
R = 1.987 CAL/MOLE-DEG
8000 °K
10,000 °K
4000 °K
6000 °K
0.1 ATM
1
10
50
100
PERCENT CARBON IN MIXTURE

Figure 16

(made of copper) contribute trace quantities of vapor. Trace amounts of copper significantly affect the electrical conductivity resulting in the lowering of the gas enthalpy and efficiency of the arc generator. Estimates of the effects of carbon contamination can be made (44). Concern for the role of contamination has also stimulated exploration of arc geometries and techniques of inherently low contamination.

Thus a tandem Gerdien (divided flow type) arc heater has been developed by McGinn (47) which affords a moderately high Mach number air-arc wind tunnel of high purity (Figure 17). The end chambers are the anode and cathode housings; a portion of the entering air blows through these housings, mixes with the carbon eroded from the electrodes and exhausts from the system. The test air is heated in the arc column and collected in the plenum located at the center of the unit. The gas is then expanded through the sonic throat and the conical nozzle to the test section. The test section is of the flow jet type with the models mounted downstream. This geometry presently provides clean flows of air at stagnation enthalpy values (h_s/RT_o) of the order of 400 with running times of up to 15 minutes duration. A continuous operation in excess of one hour is expected. Spectroscopic studies of the gas exhausting from the plenum have shown it to be free of contamination to the order of 100 ppm at these conditons (33).

The materials data discussed in this paper however were obtained in more conventional geometries with contamination levels of 4% or less except where stated otherwise.

6.2 Models

The models and materials used in this investigation are given in Figures 18, 19, and 20. With the exception of the quartz specimen, models are generally constructed from two pieces. Actual test specimens, except for quartz, are 1/4 inch diameter slug inserts into a base model of the same material. Use of inserts enables accurate stagnation weight loss measurements to be made which can account for losses due to pyrolysis and charring.

A useful measure of the heat protection effectiveness of material of varying elements can be obtained from weight depth defined as the product of the density of the material by the length of the specimens. Weight depths used herein are given in Table 2.

6.3 Low Heating Rate Results (30, 31)

6.3.1 Surface Temperature

Surface temperature histories at the stagnation point and skirt position for three materials tested are shown in Figure 21. These results were obtained from total radiation measurements made with a Golay cell used in conjunction with the constant emissivity values shown in the figure. The assumed emissivities are probably satisfactory for determining the temperatures of the two charring plastic materials, phenolic nylon and polyurethane; since the emissivity of Teflon is small, however, an error in the assumed value could cause the T_{Su} values to be inaccurate to perhaps 15% or 20%. An assumed value of .15 gives a temperature in reasonable agreement (7%) with that predicted by Scala (27). The Teflon data is interesting in that it provides an indication of the steadiness of the ablation process. For the stagnation point case, the surface temperature rises to 95% of its maximum value within the response time of the Golay cell (as predicted in the theoretical results). However, at the skirt position it takes approximately 70 seconds to reach the 95% point. This may be associated with significant non-steady effects at the skirt.

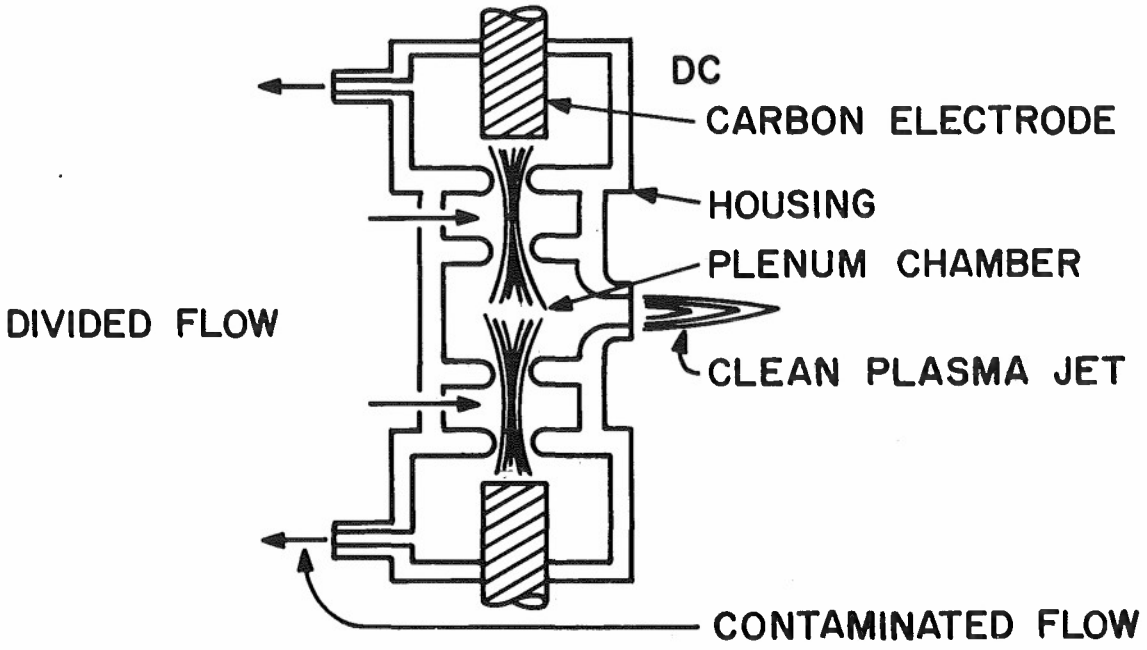

Figure 17. Tandem Gerdien Plasma Jet

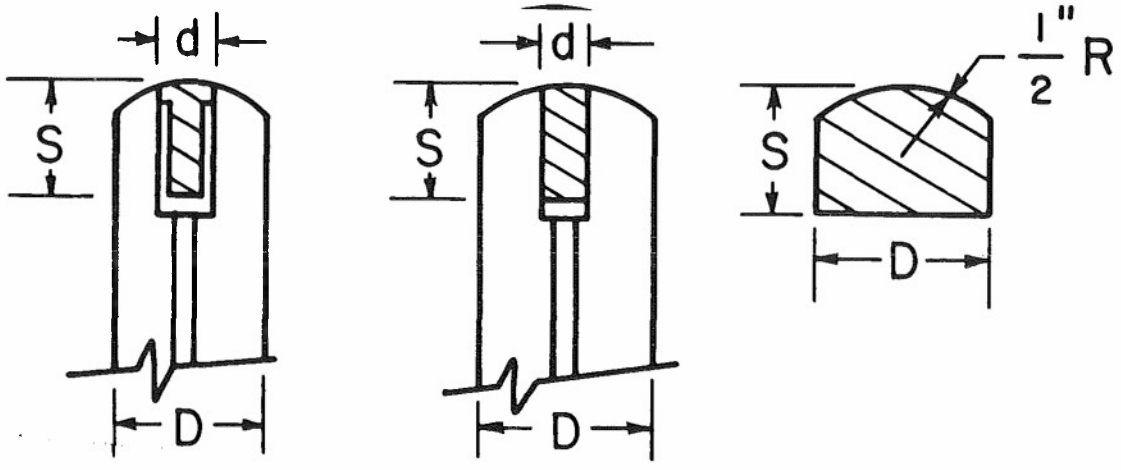

* PHENOLIC NYLON

MATERIAL	THERMOCOUPLE LOCATIONS	SPEC. GRAV.
TEFLON	S = .500"	2.21
QUARTZ	.500"	2.20
GRAPHITE	.608"	1.82
*PHENOLIC NYLON	.906"	1.22

*(38-40) % RESIN BY WEIGHT
D = .667" DIA.
d = .250" DIA.

Figure 18. Sketch of Model Specimens

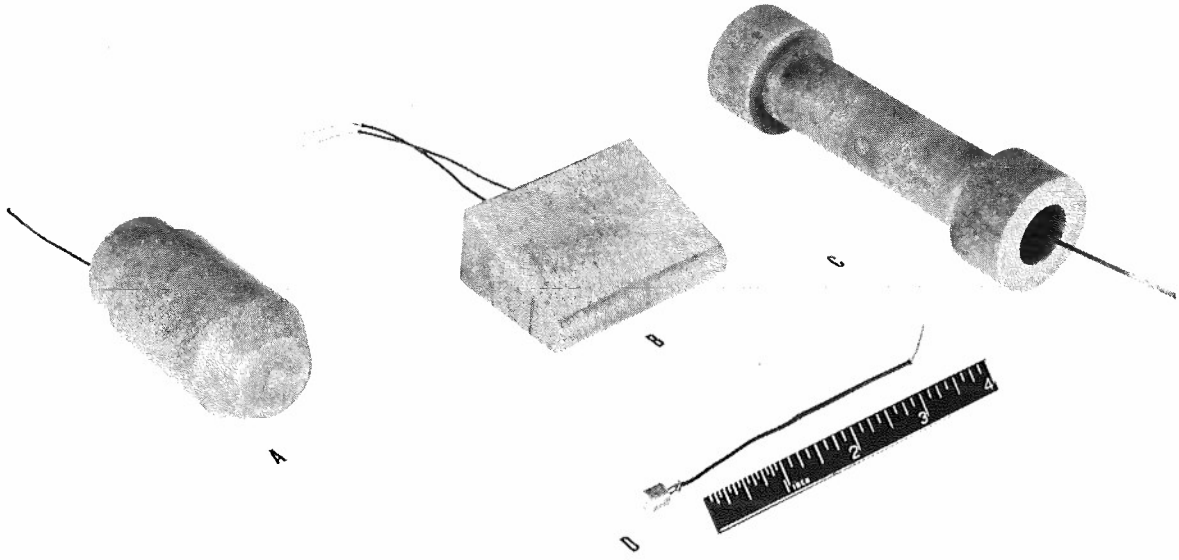

Figure 19. Test Models and Specimens:Phenolic Nylon

A. Stagnation Point Model
B. Skirt Model
C. Variable Heating Model
D. Copper Calorimeter Slug

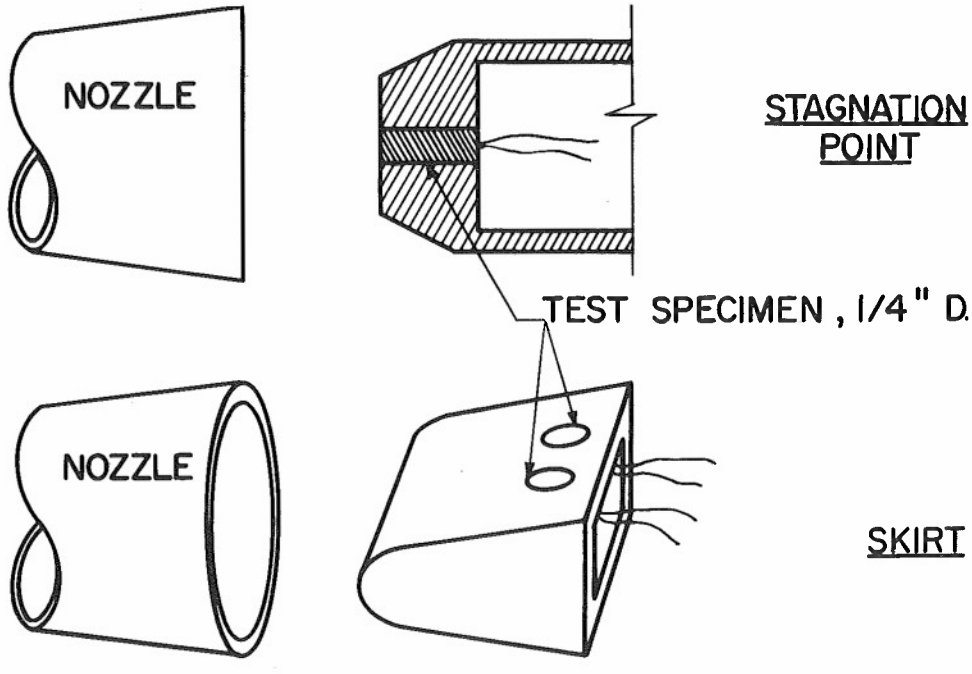

Figure 20. Test Configurations

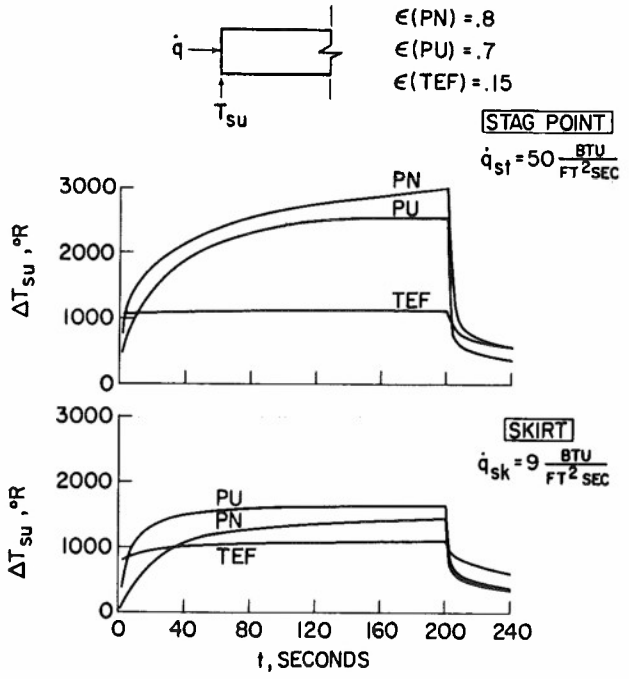

Figure 21. Surface Temperature Histories

TABLE 2

WEIGHT DEPTHS OF MATERIAL USED

Regions	Weight Depths lbs/ft^2	Material				
		Teflon	Phenolic Nylon	Polyurethane	Quartz	Graphite
Stagnation δ_1	4.28	*	*	*		
δ_2	6.43	*	*			
δ	5.78	*	*		*	*
Skirt δ_3	1.29	*	*	*		
δ_4	1.93.	*	*			

Non-steady ablation effects also appear in the surface temperature data for phenolic nylon and polyurethane at both the stagnation point and the skirt locations. The polyurethane reaches a steady surface temperature in about half the test time whereas the phenolic nylon curve is still rising at the end of heating. The shapes of the curves for each material are qualitatively similar at the two test locations; their relative positions reverse, however, the maximum temperatures being exhibited by phenolic nylon at the stagnation point and by polyurethane at the skirt. There is thus an appreciable effect of $\dot{q}$ on the general surface temperature levels and, therefore, on the ablation characteristics of the charring plastic materials at the test heat transfer rate levels. This is not unexpected, since, as pointed out by Scala (27), the mass evolved in a constant stagnation enthalpy environment will determine the surface (or char-plastic interface) temperature; a reduction in the heating rate will cause a reduction in the mass loss rate which in turn will reduce the surface temperature.

The drop in surface temperature, after the test flow is terminated, is also shown in Figure 21. The high emissivity, high temperature materials quickly radiate away large amounts of heat and their surface temperatures drop rapidly below that of Teflon. Recording of surface temperatures after t = 240 seconds was not practical because of the low signals given by the Golay cell.

An interesting observation can be made concerning the nature of the ablation process for the charring materials. The rate at which heat is radiated away from the phenolic nylon stagnation point towards the end of the heating cycle, for example, is approximately 63 Btu/ft^2 -sec. This is actually a larger value than the calorimeter heat transfer at the test conditions. Since it is obvious that heat is transmitted into the material as well, it is apparent that a large heat source exists near the surface of the material. Thus, it would appear that a major influence on the ablation of such materials is provided by exothermic processes (primarily combustion) occurring near the surface. This fact causes difficulty in defining the heat of ablation of such a material in the environment considered, since this quantity usually includes the radiated $\dot{q}$ term. Even if the radiation term were eliminated from the definition, the strong variation in surface temperature during ablation would force additional artificiality into the concept. Thus it is useful to state mass losses from which heats of ablation may be calculated.

6.3.2 Backwall Temperature

Backwall temperature histories at the stagnation point and skirt region are given in Figures 22 and 23. Comparison of the shapes of the curves in the early times of the test runs leads to interesting conclusions concerning the non-steady nature of the ablation process. For example, in Figure 22 the weight depths at the skirt are 30% of the corresponding value at the stagnation point while the heat transfer rate has been reduced to 18%. Temperatures for Teflon and nylon rise to a higher value at the skirt than at the stagnation point. This suggests that the heat protection afforded by mass transfer is less at the skirt than at the stagnation point. This may also be seen from the steepness of the backwall temperature curves during ablation ($t < t_q$) and the relatively slow rise of surface temperatures early in the ablation period (Figure 21) for these two materials at the skirt position. It is concluded that for Teflon and phenolic nylon, in the early phases of the heating period, the behavior is more typical of a heat sink than of an ablating material at the skirt position. Once the ablation process has been established, during the second half of the heating cycle, which is indicated by the leveling off of the surface temperatures, the heat protection improves and the slope of the backwall temperature curve begins to drop. The polyurethane skirt response, however, is similar to that observed at the stagnation point, and the backwall temperature histories are about in the proper relation to each other considering the reductions in $\dot{q}$ and δ from the stagnation point to the skirt.

6.3.3 Temperature Comparison with Theory - Teflon (Section II)

A comparison of experimental and analytical results for surface temperature is given in Figure 21. Since the theory is based upon semi-infinite slab conditions, a short test series was conducted with test specimens that effectively simulated this situation. Thermocouples were imbedded within the specimen at the same weight depth locations used earlier for the finite thickness wall stagnation point tests. The agreement of the surface temperature during ablation with the theoretical prediction is fairly good during ablation and very good during cooldown. The shapes of the plotted data points agree quite well with the theoretical predictions at both ℓ_1 and ℓ_2; however, the theory overestimates the data at ℓ_1, and underestimates it at ℓ_2. Two effects could be

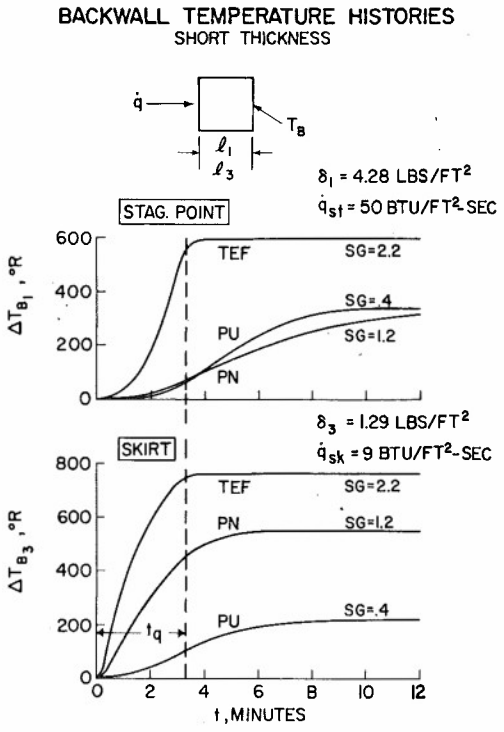

Figure 22

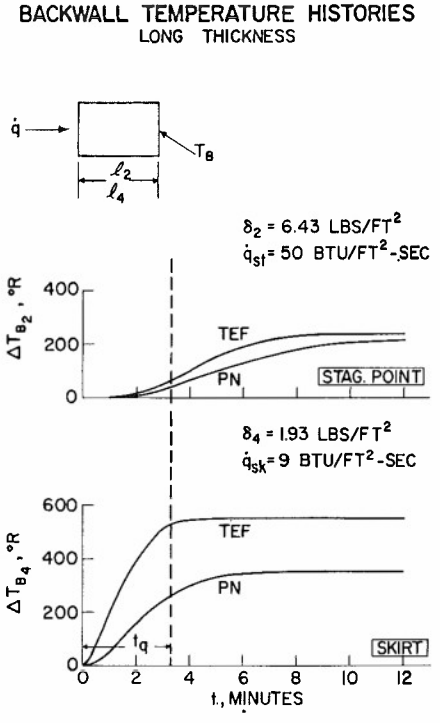

Figure 23

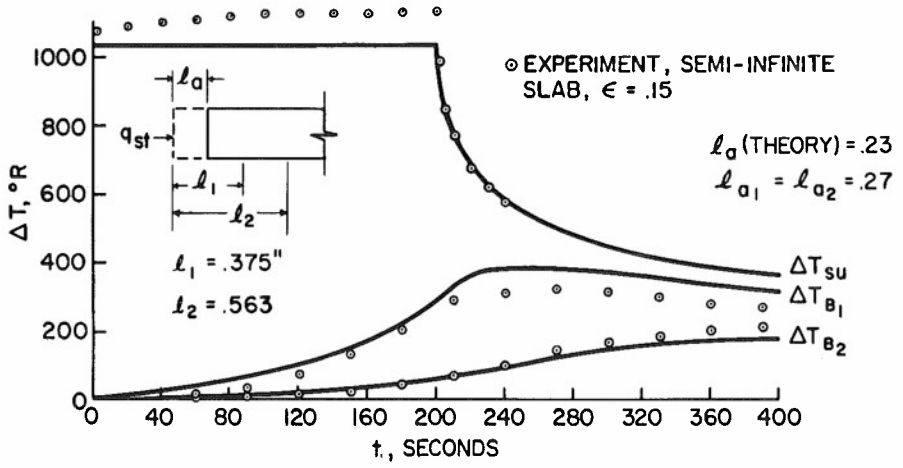

Figure 24. Comparison of Experiment and Theory for Teflon at Stagnation Point

contributing to this behavior. More mass loss was observed experimentally than was predicted; this would result in an increased blockage of the aerodynamic heating and, therefore, a reduction in heat transferred through the material. Alternately the model dimensions were such that ℓ_2 is reasonably close to the rear surface, thus a higher temperature would be expected there than at the same point in a true semi-infinite slab.

The resultant equilibrium temperature for finite thickness walls can also be obtained from the theoretical analysis and may be compared with the stagnation point Teflon data given in Figures 22 and 23. The analysis predicts final temperature levels of 725°F and 320°F for ℓ_1 and ℓ_2 while the observed values are 650°F and 300°F, respectively. This overestimation of the data by the analysis could again be in part caused by the larger experimental mass loss giving better heat blockage. Variations of the thermal properties of Teflon, which are not really negligible for the temperature ranges of interest, could also be responsible for some of the difference observed between experiment and theory for both the semi-infinite and finite wall cases.

6.3.4 Mass Loss

Table 3 gives average integrated mass losses obtained at the stagnation point and at the skirt position. In going from the high heat transfer rate position at the stagnation point to the low heat transfer rate position at the skirt ($q_{Sk} = .18\ q_{St}$), the reduction in mass loss for phenolic nylon and polyurethane approximates the reduction in heat transfer rate; the mass loss for Teflon, however, drops to only 7% of its stangation point value at the skirt. This may in part be due to the fact that some flow of Teflon was observed on the surface of the skirt models, generated apparently at the higher heat transfer rate regions upstream of the test specimens. The tendency of Teflon to exhibit heat-sink properties during part of the heating cycle, as discussed earlier, could also be responsible for the low value of $\dot{m}$ at the skirt position. Several theoretical predictions of $\dot{m}$ (discussed

in Section II) for Teflon at the test conditons are included in Table 3. Only one theoretical point (51) considers transient conditions - the others assume a steady state response. The general agreement of the experimental result with theoretical predictions at the stagnation point would indicate that Teflon is undergoing primarily steady stage ablation at that body station. Similarly, the disagreement of experiment with theory at the skirt suggests the existence of important non-steady effects there.

It is interesting to compare the total mass losses and final temperature in the different weight depth tests for the same materials at the same model locations. First, it is observed that the measured mass losses are independent of the weight depth; this implies that the response of the material, whether it exhibited steady or non-steady ablation characteristics, did not depend upon δ (or, therefore, on the subsurface temperature distribution) at least for the range of values considered. This conclusion is supported by the final Teflon equilibrium temperature levels which show that approximately the same quantity of heat was absorbed by the remaining material (when the variation of the specific heat of Teflon with temperature is taken into account). Now, a comparison of the final temperature levels and remaining mass values for phenolic nylon allows the determination of an effective specific heat ratio for both weight depths. It is found that the effective specific heat of the short specimen is approximately 17% larger than that for the long specimen. This increase is probably caused by the larger percentage of damaged (charred, pyrolized) material in the shorter specimen.

Experimental values of Q^* for Teflon and phenolic nylon are shown in Figure 25. These results are for a stagnation enthalpy (h_s/RT_o) of 125, a model stagnation pressure of 0.02 atmospheres, and a heating pulse of 69 B.t.u./ft.^{2}-sec., ($T_w = 660^oR$). Testing times of 120 sec and greater were used in order to expose the materials to total integrated heating commensurate with re-entry satellite environments. The linear theoretical behavior is also indicated (27, 22, 30).

Since the heating cycle of the re-entry trajectory of a satellite is long, it is important to consider thermal insulation properties. To examine these characteristics at low heating rates, the specimens were exposed to a square heat pulse for a two minute period after which the facility was turned off and the models were allowed to cool down at evacuated conditions. Under these circumstances, heat loss is primarily by radiation; the convective and combustion processes, (not simulated), that would normally occur during actual re-entry tend to oppose each other, permitting at least some insight to the insulation problem to be obtained from such tests. In Figure 26 typical temperature profiles are given.

Examination of the heat of ablation of Teflon at low heating rates shows the data on the average to be about 20 percent higher than the theory mentioned in Section II (Ref. 27) for a stagnation enthalpy ratio of 125. Namely, the expected increase in Q^* with decreasing stagnation pressure, (Figure 5) also appears to be indicated in the experimental results.

The theoretical calculations of Scala (of Section V) for Q^* of phenolic nylon were used along with the experimental data to infer a material surface temperature. The experimental results in Figure 25 for Q^* represent a reduction of the data assuming a surface temperature of 2500^oR.

TABLE 3

INTEGRATED MASS LOSSES

Stagnation Point $\dot{q}_{St}$ = 50 Btu/ft^2-sec Q_{St} = 10,000 Btu/ft^2

h_s = 5900 Btu/lb

	m (av. exper.) lbs/ft^2	m (other sources) lbs/ft^2
Teflon	3.15	2.58 Georgiev, etc. (12) theory 2.90 Georgiev, etc. (12) exp. 2.89 Sutton. theory (Section II and (51)) 3.30 Scala (27) theory 2.89 Scala, Diaconis (30) exp. 2.69 Transient, 3.09 Steady } Sutton (51)
Phenolic Nylon	1.38	
Polyurethane	3.34	

Skirt $\dot{q}_{Sk}$ = 9 Btu/ft^2- sec Q_{Sk} = 1800 Btu/ft^2

h_s = 5900 Btu/lb

	m (av. exper.) lbs/ft^2	m (other sources) lbs/ft^2
Teflon	.213	.524 Aver. for refs. (12), (27), (51) and Section II
Phenolic Nylon	.238	
Polyurethane	.523	

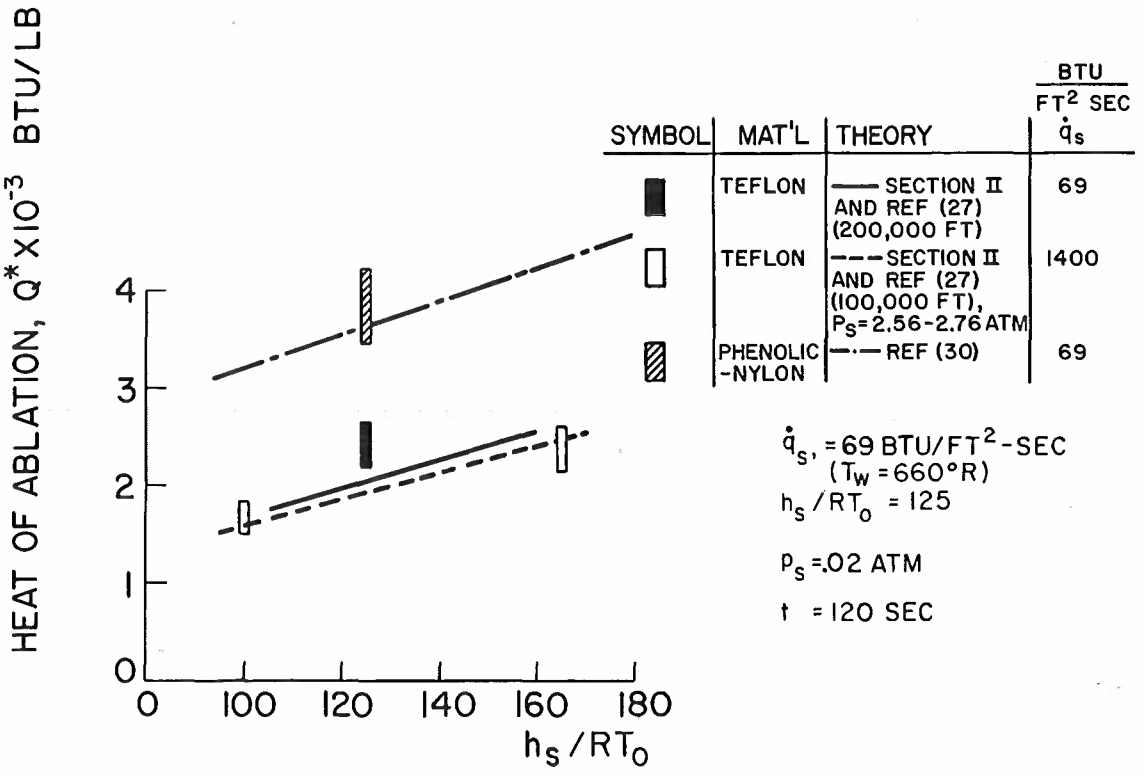

Figure 25. Experimental Heats of Ablation at Low Heating Rates

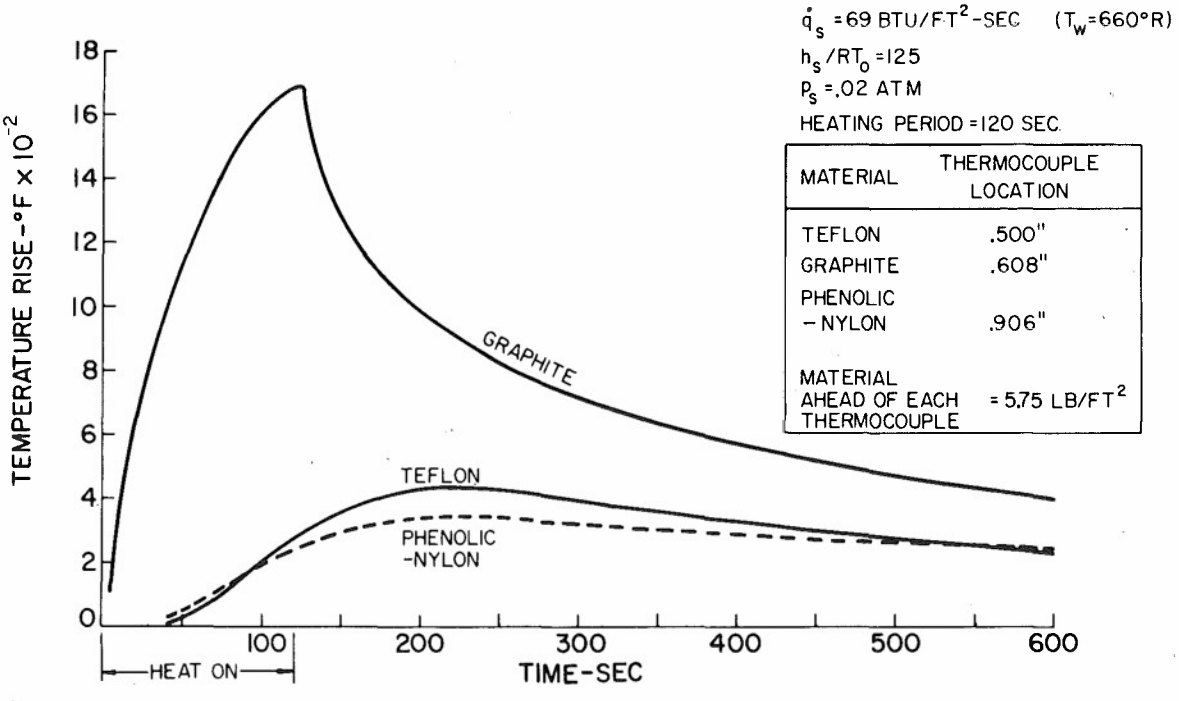

Figure 26. Relative Backface Temperature Rise in Materials - Low Heating Rates

6.3.5 Models After Test

Photographs of models after test are shown in Figures 27 and 28. Three stagnation point models are shown in Figure 27. The surface of the cylindrical sections showed little or no effects of heating. For polyurethane, the char remaining on the front surface was an integral part of the parent material. The Teflon surfaces were clean and actually smoother after test than before. The highly porous loose char formed on phenolic nylon was easily removed from the base material.

A phenolic nylon skirt model is shown in Figure 25b. The difference in the char structure in the high and low heat transfer rate environments is seen in this photograph. For both positions, the affected surface in the in the material can be divided into two regions: loose char, and a damaged layer which remains an integral part of the base material (Figure 27b).

Except for the fine indications of flow on the wedge models, the Teflon models showed no unexpected effects. However, it has been observed in earlier studies that Teflon models of certain shapes after being exposed to long time, low heating rate environments, will go into a plastic state and deform under their own weight.

Figure 28 shows cross-sectional views of two phenolic nylon models after two different exposure times. As expected, considerably deeper penetration is apparent in the specimen subjected to the longer test.

6.4. High Heating Rate Results

The performance of Teflon and quartz at high heat transfer rates is shown in Figures 29 and 30 (30). Stagnation pressure was essentially constant at about two and one half atmospheres absolute, while the calorimeter heating

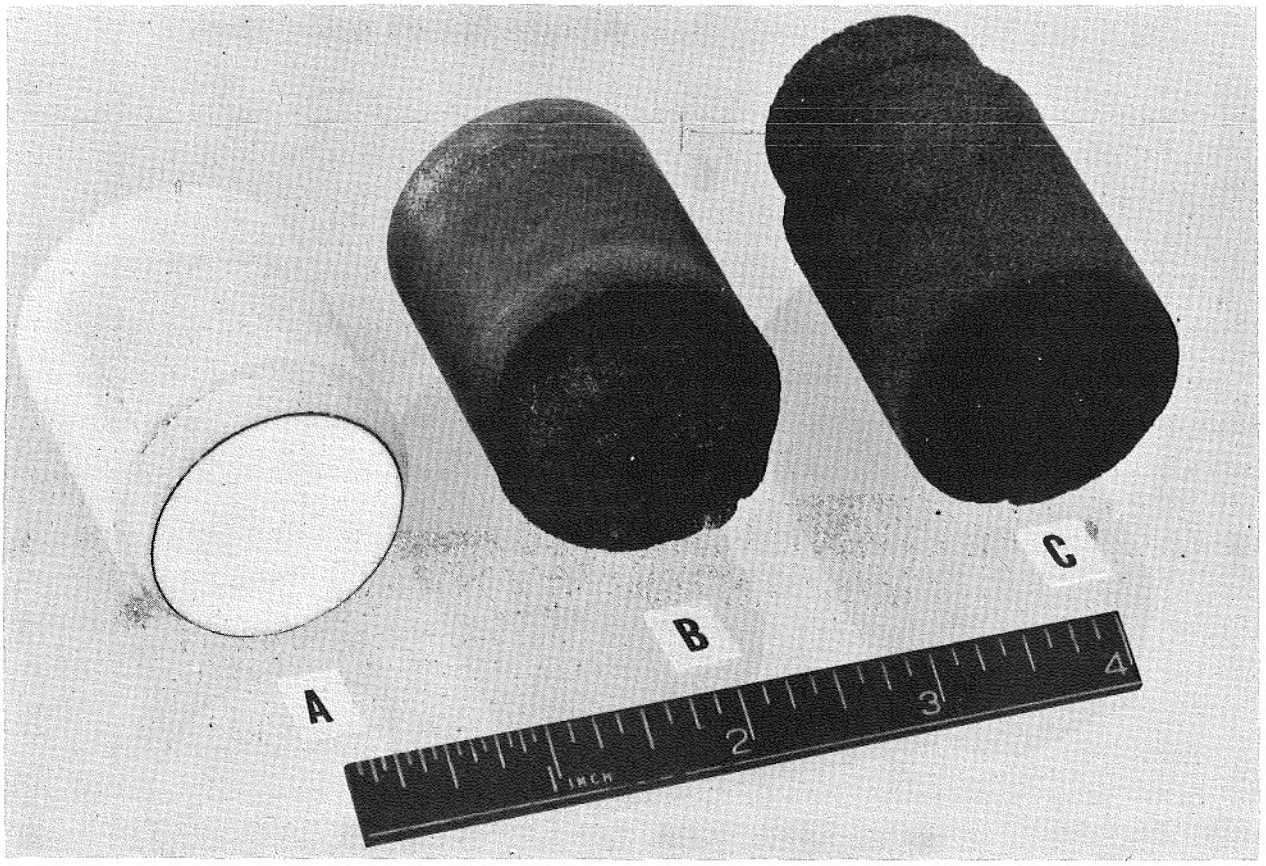

Figure 27a. Stagnation Point Models After Test (Low Heat Flux) A. Teflon, B. Phenolic Nylon, C. Polyurethane

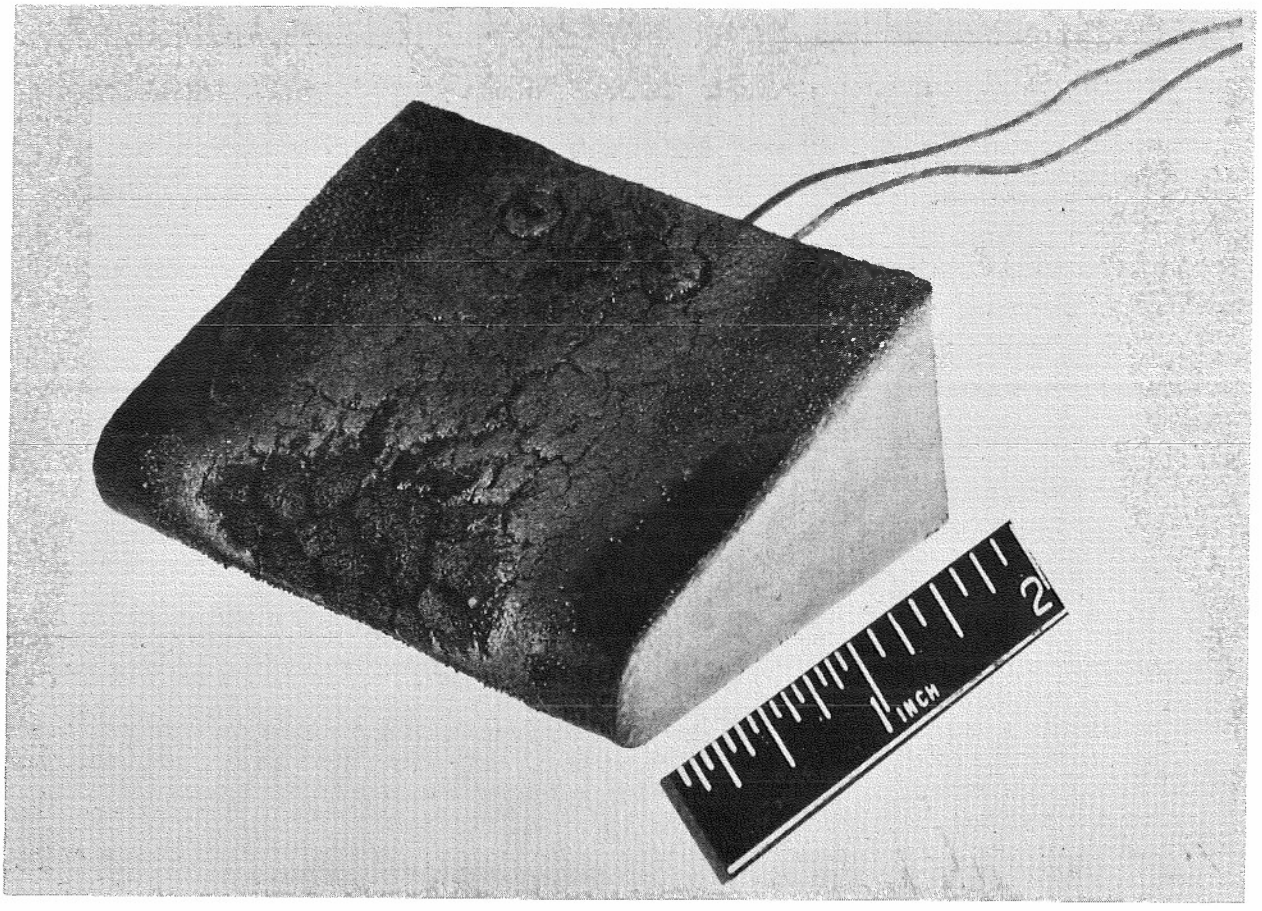

Figure 27b. Skirt Model After Test Phenolic Nylon (Low Heat Flux)

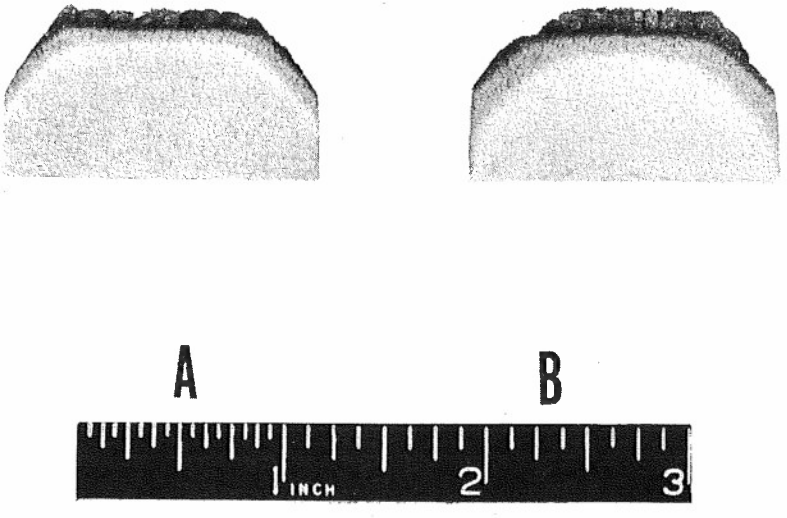

Figure 28. Damage Penetration-Phenolic Nylon- $\dot{q}$ = 50 Btu/Ft^2-sec
A. 1000 Seconds B. 200 Seconds

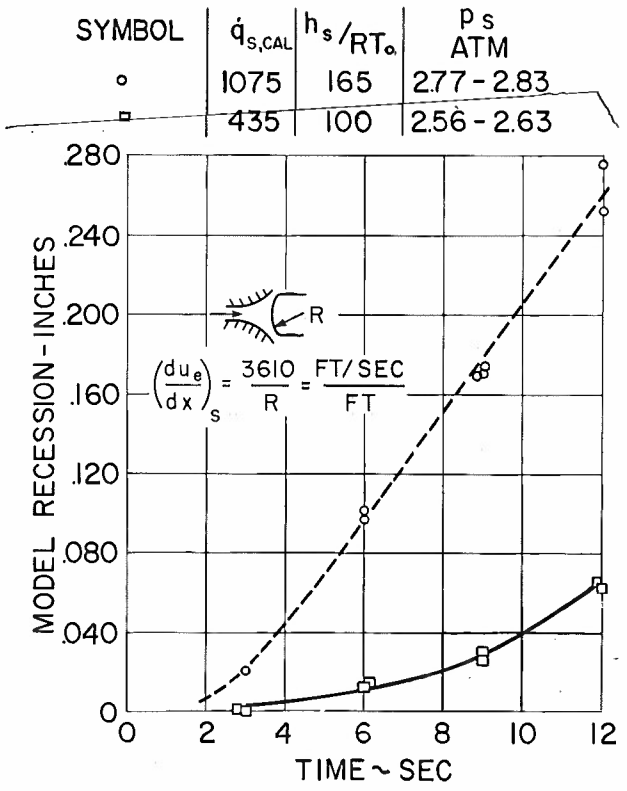

Figure 29. Stagnation Point Ablation of Transparent Fused Quartz

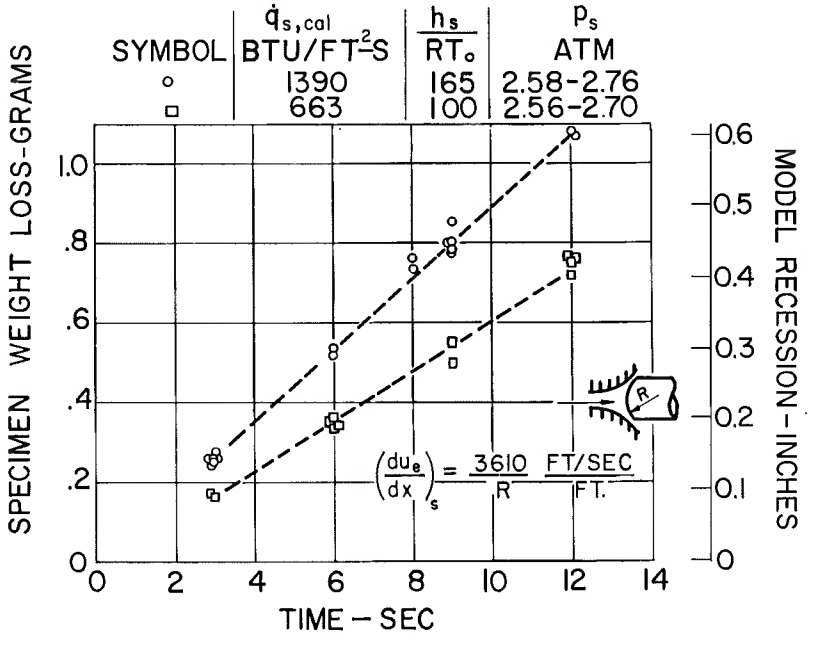

Figure 30. Stagnation Point Ablation of Teflon

rate was varied from 435 to 1390 Btu/ft.^{2}-sec. as the stagnation enthalpy (h_s/RT_s) was increased from 100 to 165. (Calorimeter heating rate is defined as the heat transfer rate to a non-ablating surface at the temperature of the ablating model.) Mass loss lag, due to heat-sink behavior and in accordance with relative heat capacity, occurs as expected. The experimental heats of ablation (Figure 31) at the high heating rates for both the Teflon and the transparent fused quartz show good agreement with the calculations of Scala (27) and Fanucci (30) , and exhibit the predicted rising trend as the stagnation enthalpy is increased. Calorimeter heat transfer values and radiation effects were calculated based on a theoretical determination of surface temperature for both materials. An emissivity of 0.1 was used for the reduction of the quartz data.

Measurements of backface surface temperature at the higher stagnation enthalpy condition for Teflon resulted in a 100°F rise when the material was exposed to a heating rate of 1390 Btu/ft.^{2}-sec. for a period of 9 sec. Similar tests with graphite, for equivalent specific weight inserts, indicated a temperature rise of approximately 2300°F at the nine second period. Although graphite's high thermal conductivity results in a behavior to a large extent as a heat sink at these enthalpy levels, considerable success is now being attained in materials modification whereby alterations to the thermal conduction characteristics of this material have been evolved (pyrolytic graphite). Because of such advances, graphite, with its low ablation, could assume an increasing role in very high speed entry designs.

Some recent results (33) on graphite combustion have been obtained in an arc tunnel driven by a Tandem Gerdien arc heater, which provides clean flows of air at stagnation enthalpy values (h_s/RT_o) of the order of 400 with running times up to 15 minutes duration. Spectroscopic studies performed on the gas exiting from the

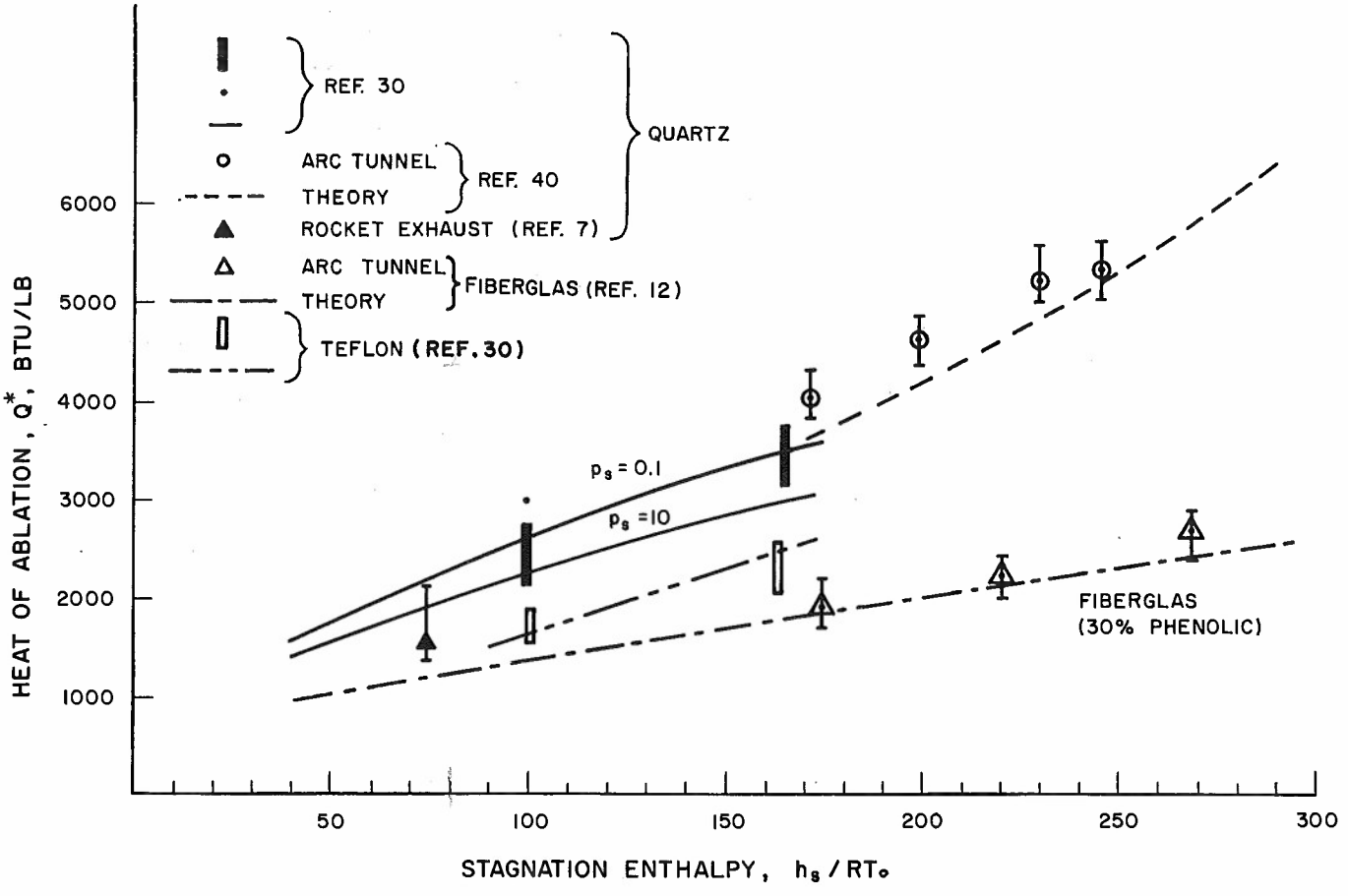

Figure 31. Heats of Ablation

plenum have shown it to be free of contamination to the order of 100 ppm at these conditions. Test results for a thin disk of graphite held in a ceramic sleeve to minimize heat losses are shown on Figure 32.

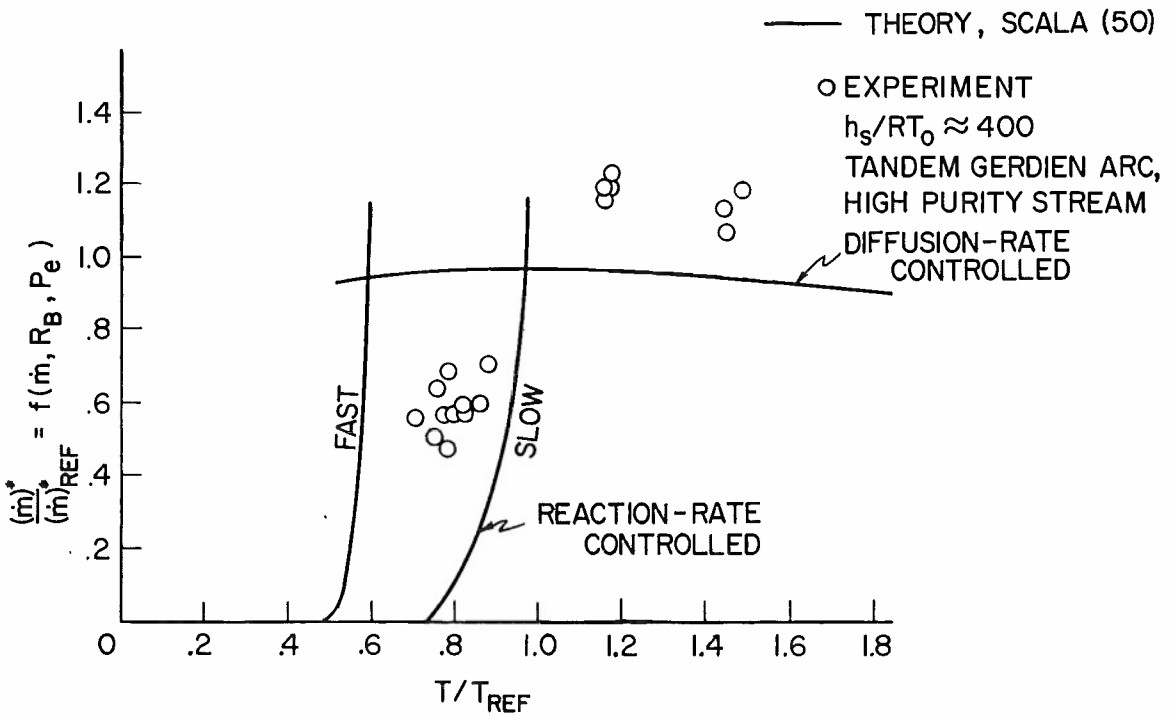

Figure 32. Mass Transfer for Graphite Combustion

6.5. Material Behavior Under Ablation Process

6.5.1 Surface and Cross-Section

Sections of models tested are shown in Figure 33. For the phenolic-glass models, a thin layer of solidified glass is deposited on the surface after the two-minute run. This layer does not form until the latter portion of the heating cycle. Thus, ablation seems to proceed in several stages. In the first part of the test, gases are being given off as a result of pyrolysis of the virgin plastic and reactions in the char layer. At some later time, a transition period is encountered during which the reinforcing material flows to the surface of the charred material and forms a fairly thick layer. After this, it is probable that the heat protection is accomplished by the release of pyrolyzed products diffusing through this layer as well as by the partial vaporization of the layer of molten reinforcing material. This phenomenological description has been verified reasonably well by photographic observations of the ablation process.

The significant variation in behavior with heating rate for some non-homogeneous materials is shown in Figure 34 for melamine glass. Total heat pulses were essentially identical; maximum heating rates differed by a factor of 14. Major differences in characteristics of the char layer are clearly evident. In the case of the low value of maximum heat transfer rate an extensive fibrous char structure of pyrolyzed plastic exists, covered on the surface by the molten reinforcing material, as noted above. In the case of the high value of the maximum heating rate the higher ablation rate clearly limited the depth of the remaining char layer, resulting in a higher mass loss, but a relatively undisturbed remaining structure.

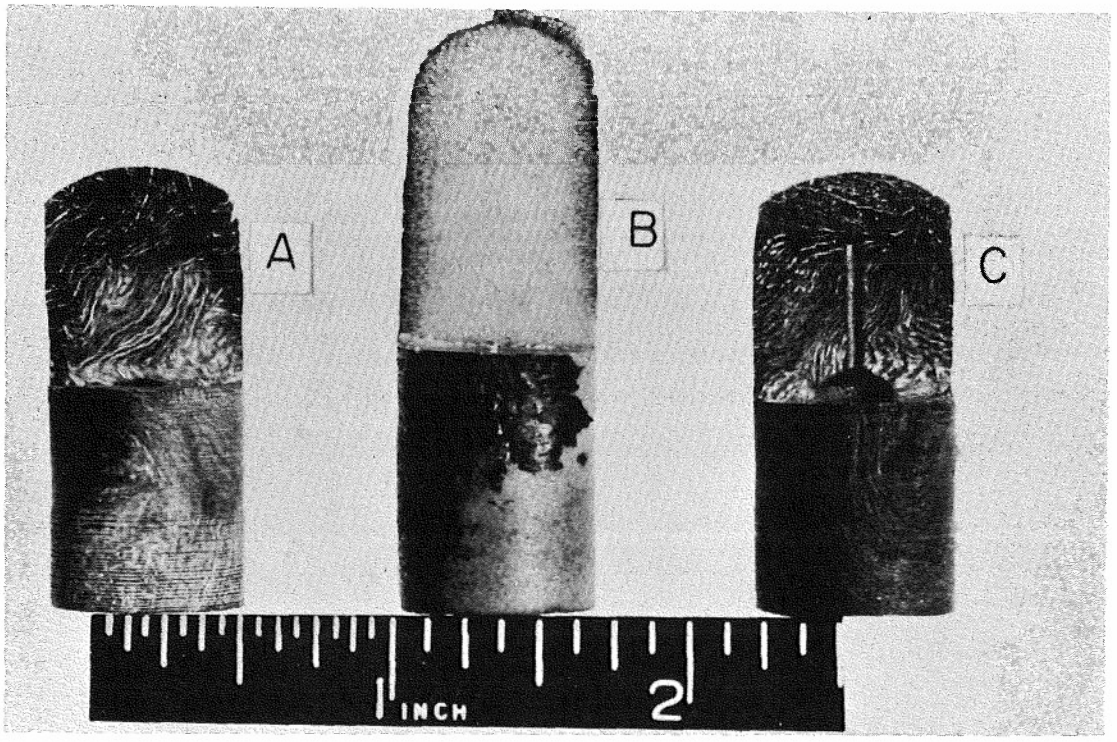

A - PHENOLIC-REFRASIL
B - PHENOLIC-NYLON
C - PHENOLIC-GLASS

$Pe = .026$ ATM

$h_e/RT_o = 150$

$\dot{Q}(\dot{m} = o) = 65 \ \frac{BTU}{FT.^2 - SEC.}$

Figure 33. Model Cross-Section - Heat Soak Study

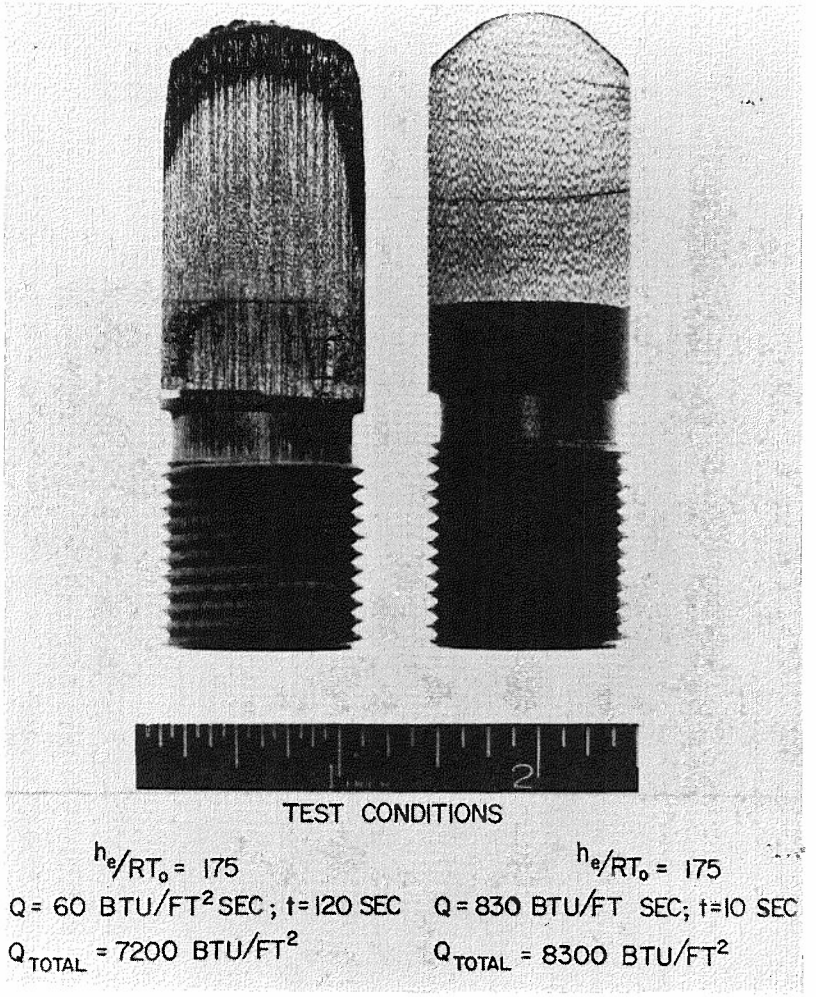

Figure 34. Comparison of Material Behavior at High and Low Ablation Rates

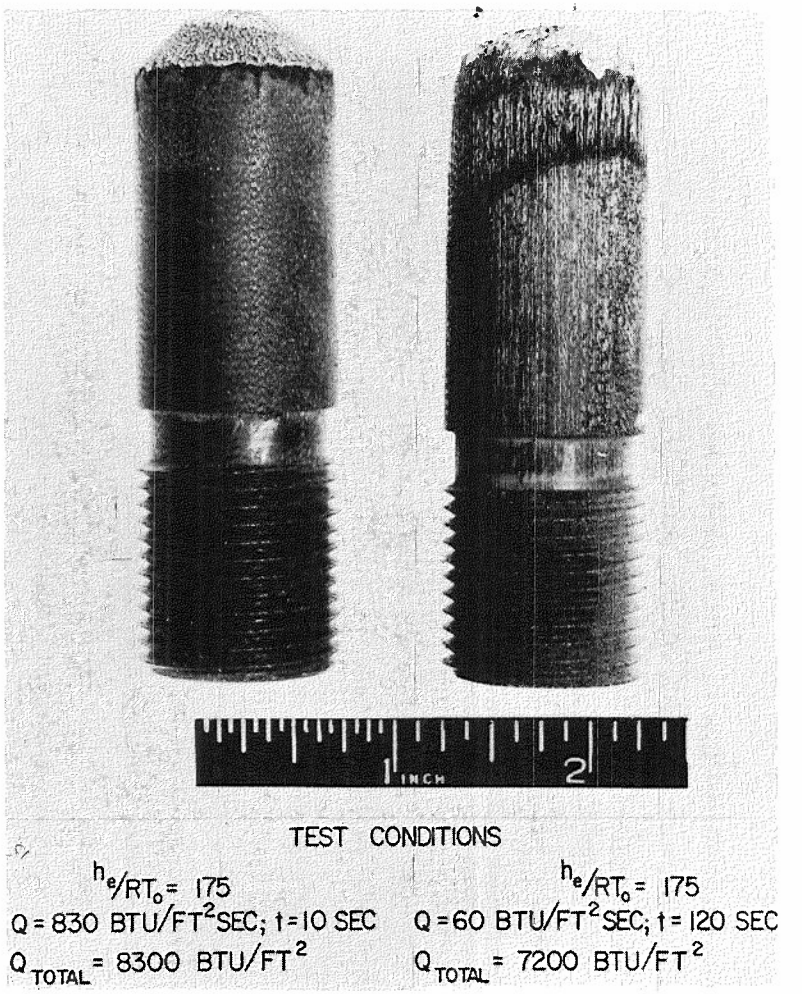

Figure 35. Comparison of Material Behavior at High and Low Ablation Rates

6.5.2 Char Structure

The function of the char during ablation has been brought out. A highly refractory barrier is formed, which is itself excellent in ablation and which may be transpiration-cooled by gases from the decomposing resin. This refractory can get very hot at the surface and radiate heat back to the surroundings. The gases percolating through this hot layer may be cracked to their lowest molecular weights and largest volumes. The additional gases, in turn, would thicken the boundary layer and thereby reduce the heat transfer to the surface. It is obvious that the chemical and physical structure of the char and its bonding to the decomposing resin interface probably plays an important role in ablation performance.

The importance of a char layer to the ablation rate of an all-organic resin system is illustrated in Table 4 (52). The ablation rate of a pure phenolic resin filled with nylon cloth, Teflon, and an epoxy resin exposed to a FSJ-3 blowpipe flame are compared. Teflon and epoxy show no evidence of char at the ablating surface and erode at 3 to 5 times the rate of the phenolic-based materials, which form chars.

Gruntfest, Shenker, and Saffire (11) have examined microscopically the char structures of an all-organic system, phenolic reinforced with nylon. They found a thin, very porous structure followed by a very narrow zone of partially pyrolyzed resin and a third region, preceding the virgin plastic, where nylon fibers had melted and flowed out.

TABLE 4

COMPARISON OF CHARRING AND NON-CHARRING RESINS

IN LINDE FSJ-3 BLOWPIPE FLAME (52).

MATERIAL	CHAR	ABLATION RATE (1/2" Dia. Cylindrical Sample)
BRP 400 Phenolic	Yes	.12 g/sec.
Molded Phenolic-Nylon 40% CTL-91 LD 60% SN 19 Chopped Cloth	Yes	.13 g/sec.
Teflon	No	.40 g/sec.
Bisphenol Epoxy cured with MNA	No	.55 g/sec.

(Heat flux - 1400 ±150 Btu/ft^2 sec., Temp. 5200°F, Mach No. M = 1.6)

A sample of an epoxy resin after exposure to a test plasma for three seconds was cut in half; the rear portion (plasma exit) is shown in Figure 36(52). The char which develops is hard and structurally continuous, forming an inner, concentric cylinder. Part of this char extends beyond the face of the sample, indicating that a plastic flow occurred. More evidence of this is shown in subsequent photomicrographs.

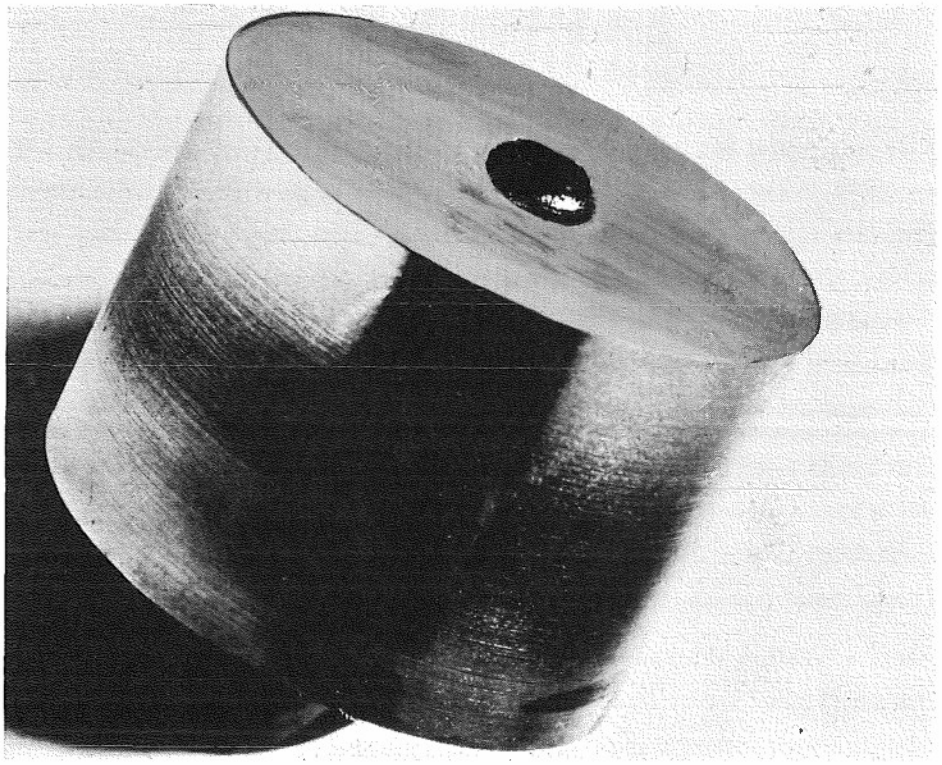

Figure 36. Sample of Cast Epoxy Resin Exposed in Air-Arc Plasma for Three Seconds

Photomicrographs of chars from a phenolic reinforced with nylon and from the resin are compared in Figure 37. These pictures were taken of polished thin-sections using both transmitted and reflected light at a magnification of twenty times. The hot plasma passed through the center of the char ring; the lighter, outer portions are virgin resin. The cracks appearing in the center of the holes are actually fissures in the epoxy impregant used to reinforce the specimens during the polishing operations. Although the phenolic nylon was exposed to the plasma for 5.5 seconds, and the cast resin for 7.5 seconds, the former material shows considerably more erosion, since both were of the same size prior to testing. It is evident that the phenolic nylon char is thin, open, and jagged due to the melting-out of the nylon reinforcement. On the other hand, the cast resin forms a thicker and relatively dense layer adjacent to the hot surface which results in superior thermal protection to the underlying material.

The degradation and char growth of the cast resin can be followed in Figure 38, which shows freshly cut surfaces (normal to the plasma flow) of samples exposed for 1, 2, 3, and 4 seconds. The eccentricity of the hole in the char ring is due presumably to the turbulent flow of the plasma.

The inner diameter of the char layer (adjacent to the plasma) increases rapidly during the first two or three seconds, and remains relatively constant with further exposure times. There is an increase in char thickness with exposure time. Its shape depends on the rate of degradation of the resin (outside diameter), on the growth and expansion of the char, and also on the erosion rate of the hot surface (inside diameter). Along with the growth of the char layer, the weight loss of the plastic specimen gives further information regarding the degradation of the resin. The rate of weight loss is very high during the first half second of exposure and then decreases sharply. This indicates that

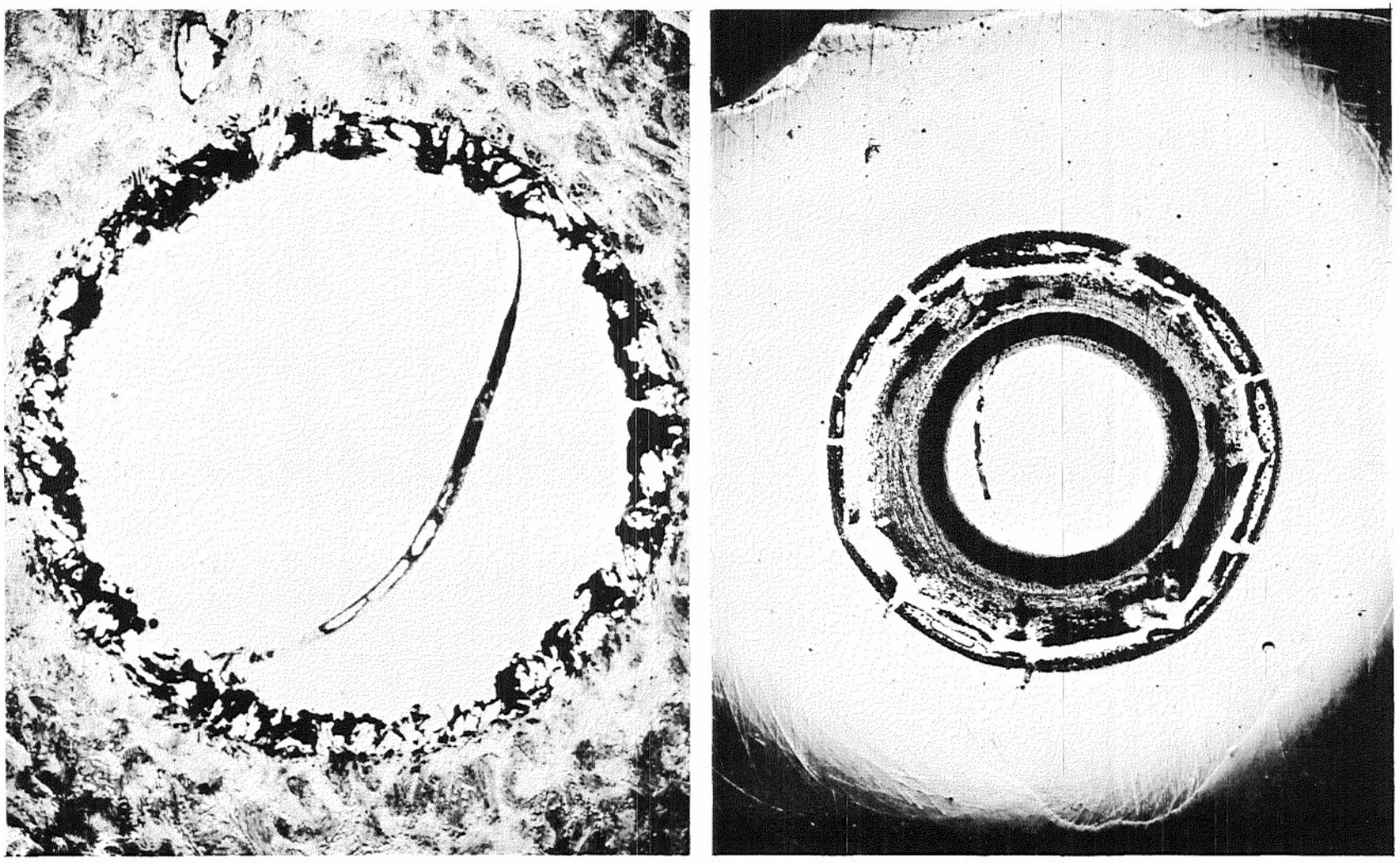

A. PHENOLIC NYLON (EXPOSED 5.5 SEC)

B. CAST UNREINFORCED RESIN (EXPOSED 7.5 SEC)

Figure 37. Photomicrographs of Chars from Phenolic Nylon and Cast Unreinforced Exposed to Air-Arc Plasma (Mag. 20X)

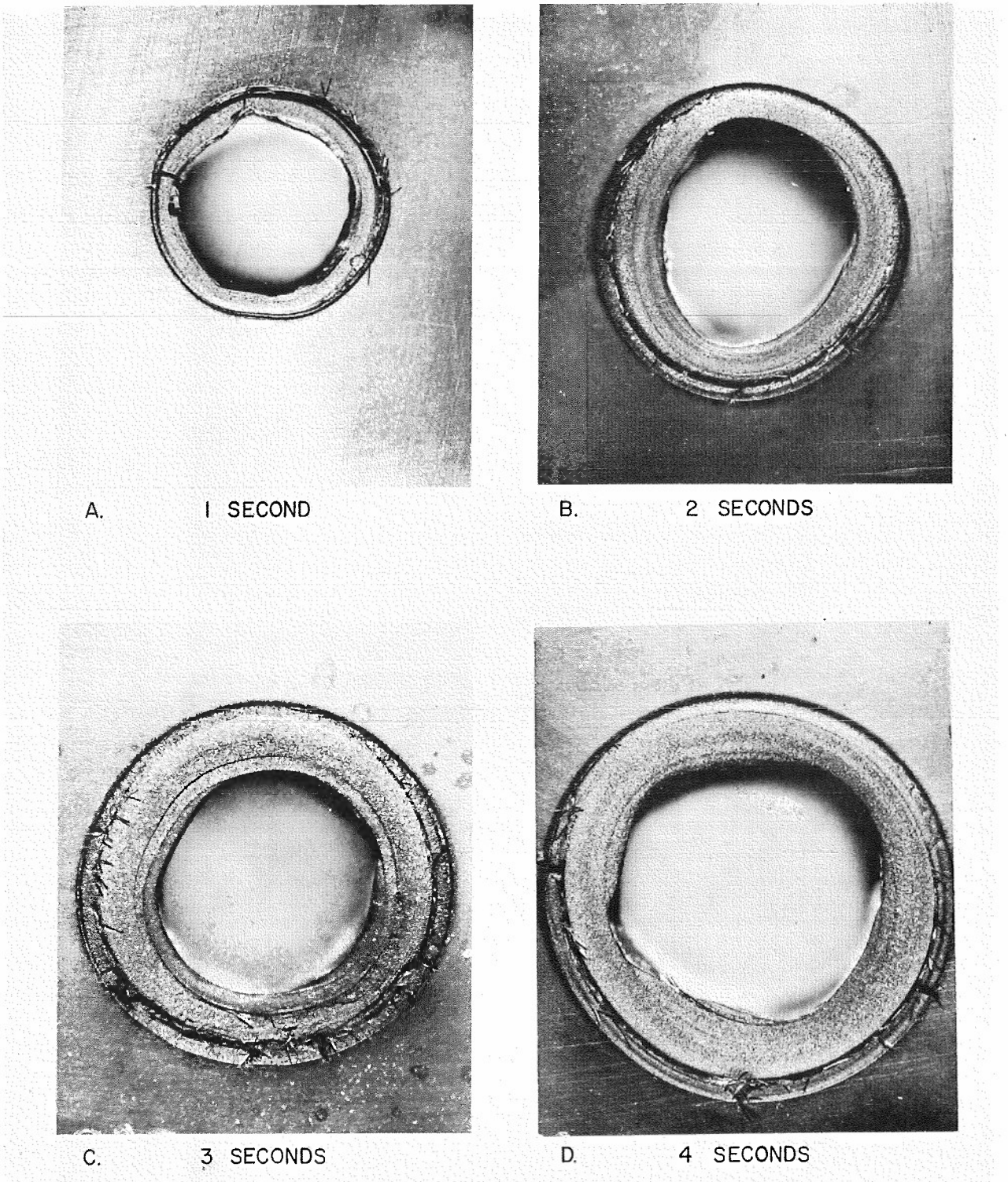

Figure 38. Increase in Char Thickness of Cast Resin Samples Exposed at Various Times in Air-Arc Plasma (Mag. 20X)

as soon as a char forms, it affords immediate protection as shown by this sharp decrease.

The char structure and thickness both play a dominant role in protecting the underlying resin from the intense heat of the plasma. In order to examine these factors better, photomicrographs of thin-sections (1/5000" thick) were taken of the cast resin samples. These samples, which were tested in the arc plasma for periods as long as 7.5 seconds, are shown in Figures 39, 40, and 41. The difference in textures and thickness of the char are readily apparent with increasing exposure times. Figure 39 shows that the char undergoes distinct structural changes as it matures.

In the photomicrographs, the upper surface of the char, which appears to be concave in Figure 39-A, C, and D, has been exposed to the intense heat of the plasma. It follows, then, that the region near the lower portion of the photomicrographs is virgin resin. This holds true for all except for Figure 39-D, where the lower region is actually a large crack (filled in with an epoxy resin) caused by an actual separation from the underlying char. These photographs give an indication of the increase in char thickness with exposure time, since they were all taken at the same magnification (100 X). Also apparent is the drastic change in char texture. The early-formed char at 0.5 seconds of exposure is fairly uniform and continuous. A fissure which developed has been partially healed or filled in. Char resulting from continued exposure to the plasma show a densification of the layers adjacent to the hot zone and show a distinct change in pore dimensions in the underlying cooler regions. This effect is most pronounced in samples exposed for 7.5 seconds, and can be seen in greater detail in Figure 40. The entire char thickness is about 0.95 inches. The pores are vesicular in the underlying layer of the char, and views taken at right angles to the section (not shown) confirms their platey nature. In fact, the pores are oriented preferentially so that their long dimensions run parallel to the sample bore. This indicates that the denser (hot) layer was not sufficiently permeable to the decomposing gases, and that they were therefore forced to escape by passing longitudinally through the pores. These changes in structure and resulting impedance to gas flow could account for the separation observed between the layers of the more mature chars.

The cellular structure of the char and changes in pore dimensions due to different thermal histories can be further observed in Figure 41. Thin-section photomicrographs were taken (1000 magnifications) of three locations within the char: (1) adjacent to the exposed plasma surface (hot zone), (2) near the center of the char (intermediate zone), and (3) adjacent to the virgin resin (cool zone). The various light and dark regions which can be seen are indicative of difference in thickness (overlapping of cells). These regions are perhaps also indicative of pyrolytic (resinoid) deposits on the carbonaceous pore walls which result from further cracking of the percolating gases. The lightest regions within the pores are actually 'open' areas where the transmitted light passes through.

If the heat were applied externally to the sample, the outer layers would periodically spall off and would continually be replaced by the underlying layers. It is evident, then, that the weight loss of the ablating cast resin is the result of two mechanisims: (1) continuous resin degradation and gas evolution, and (2) periodic spalling of the outer denser layers.

Under the test conditions used in this study, phenolic nylon forms a thin coke of very open structure which is apparently sheared away much faster than that of the cast resin. The latter forms a coke resembling a miniature open-cell polyurethane foam which grows in thickness with time. This growth is accompanied by increasing densification of the layer adjacent to the plasma, and this densification is in turn accompanied by increasing graphitization.

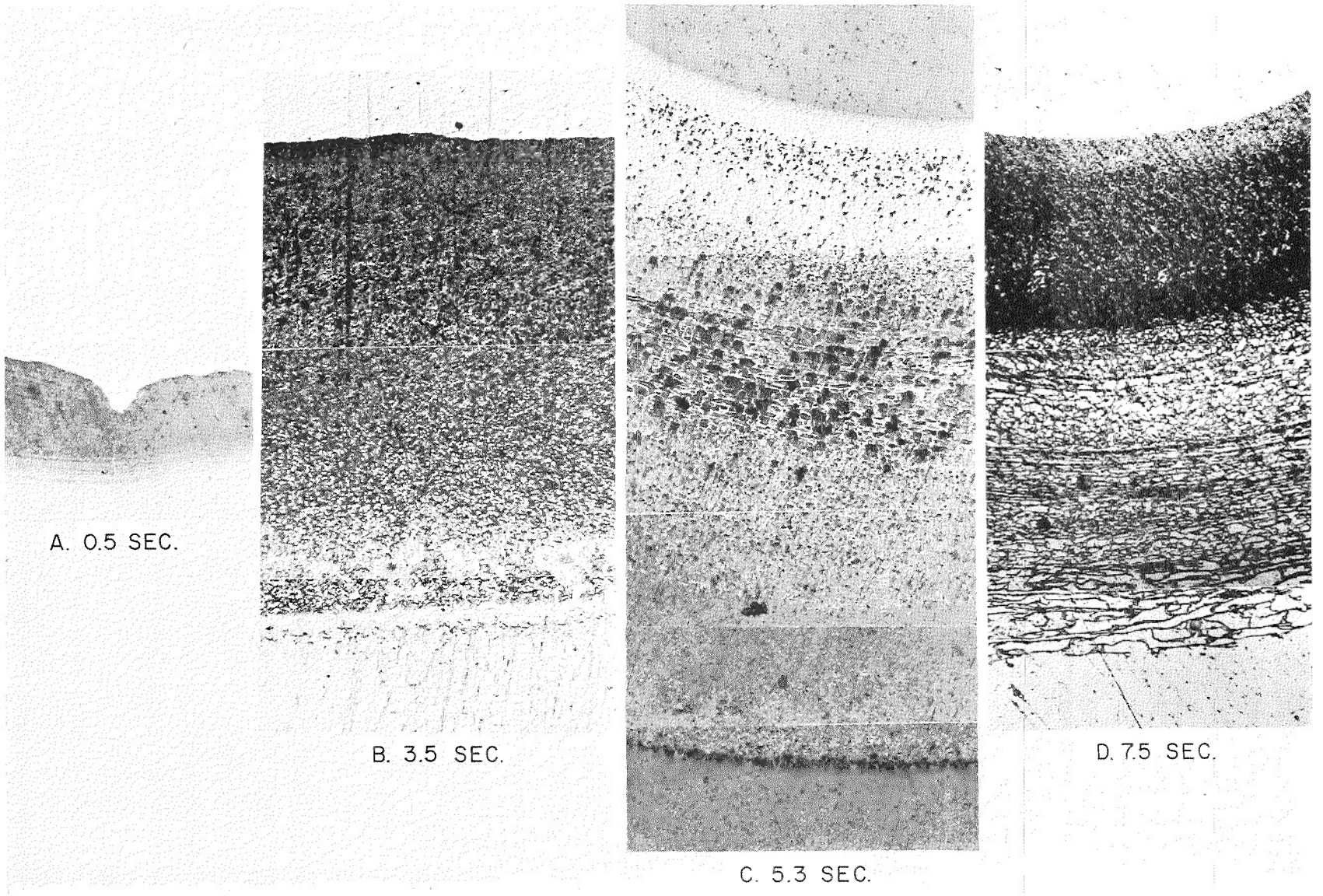

Figure 39. The Char Structures of Cast Resin Resulting From Various Exposures in Air – Arc (Mag. 100X)

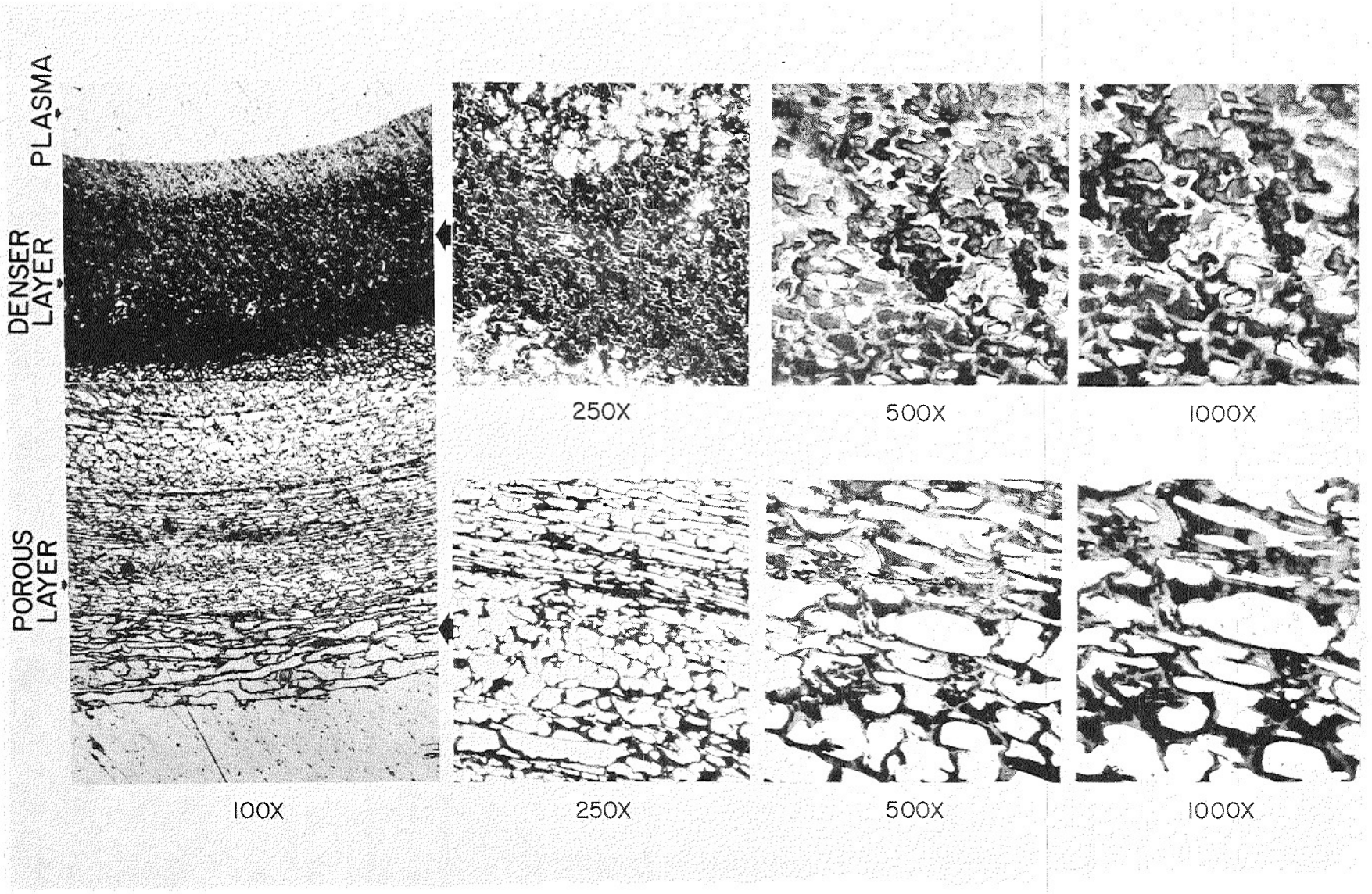

Figure 40. Photomicrographs of Char Layer Thin-Sections From Sample Exposed 7.5 Seconds in Arc Plasma

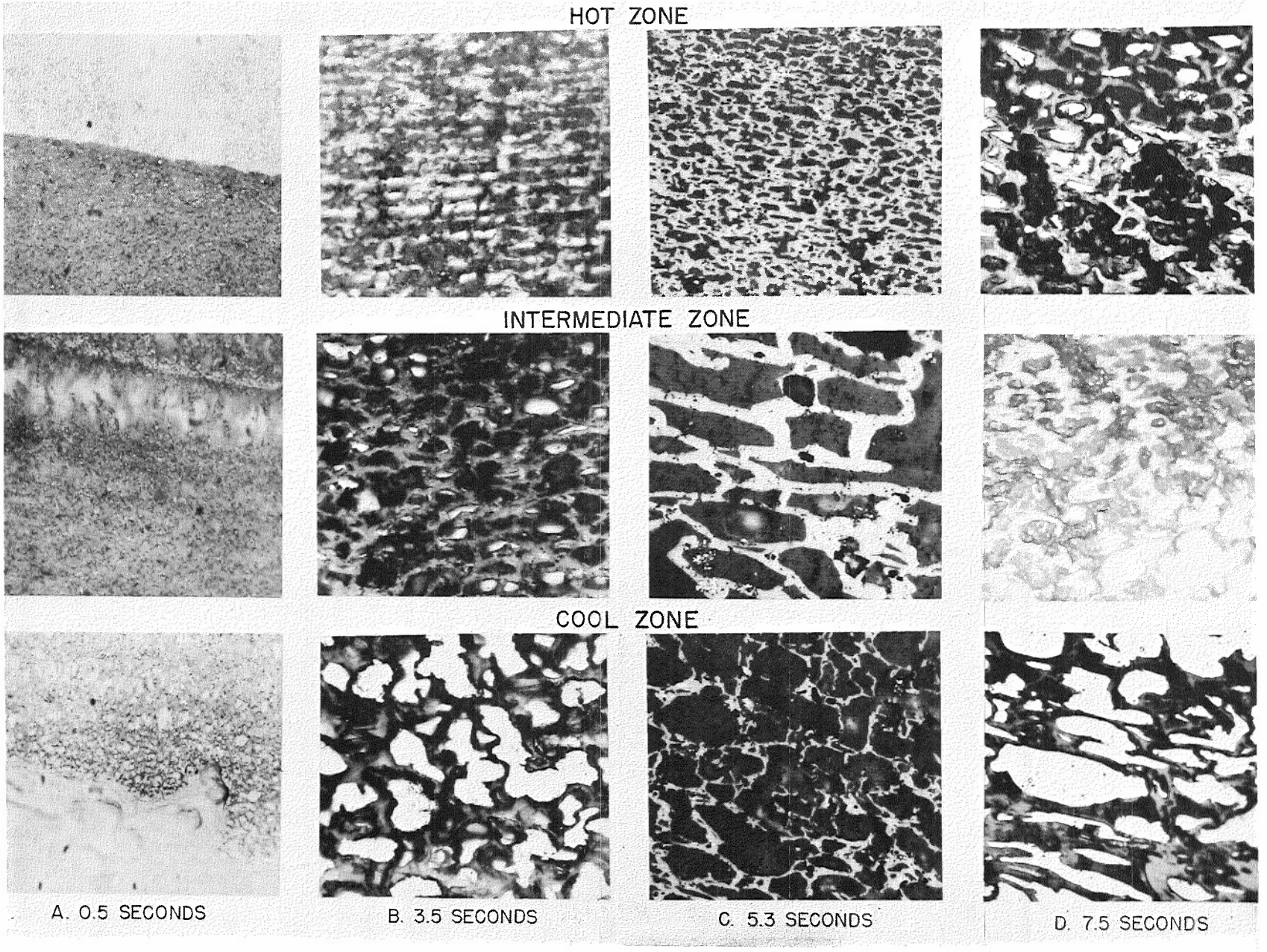

Figure 41. Photomicrographs of Thin-Sections of Samples Exposed in the Arc Plasma for 0.5, 5.3 and 7.5 Seconds (Mag. 1000X)

Cracking of the gases of decomposition could result in pyrolytic deposits on the pore walls, and is a possible cause of both densification and graphitization. Regardless of the cause, this increasing densification would impede the escape of pyrolysis products until finally the internal gas pressure exceeded the bond strength of the char resin interface, at which time spalling or separation of the char layer would have to occur. Thus, the effectiveness of the char in protecting the underlying virgin resin depends on its thickness, its structure, and also on its structural attachment during the ablation process.

A tentative model for the development and maturing of the char layer with increasing exposure times to the plasma (ca. 5200°K) of an air stabilized arc is summarized in Figure 41 (52). When the model is exposed suddenly to extreme heating conditions, rapid degradation and gas evolution results at the surface. At the degradation interface, which remains very thin (ca. 0.0007" thick), a residual carbonaceous layer is built up immediately and provides thermal protection from the intense heat. The degree of protection improves as the char layer grows and thickens. The initial or primary char which forms during the first half second of exposure is viscous. However, with further charring, it becomes sufficiently thick to entrap the escaping gas and results in the development of foamed structures (Figure 42C). This foam solidifies with further decomposition (removal of H, O, etc.), leaving a cross-linked carbonaceous structure, or secondary char. During the first four seconds of ablation, the resulting char is fairly uniform in texture, but with further exposure times, pronounced structural changes takes place. The outer (hot) surface densifies while the underlying layers expand and become extremely porous (Figure 42-E, F). The densification process impedes the flow of escaping gases and finally causes a pressure build-up in the underlying layers of the char. Consequently the pores in the interior layers become enlarged and allow the gases to pass longitudinally through the char layer. Finally the outer layers become completely detatched from the interior, porous char. Fissures into the resin which develop initially (Figure 42 B) tend to heal themselves due to the viscous nature of the char. However, fissures in the mature chars, such as those exposed for 7.5 seconds, do not heal. The extent of these cracks extending into the resin has been magnified considerably for illustration (Figure 42 F).

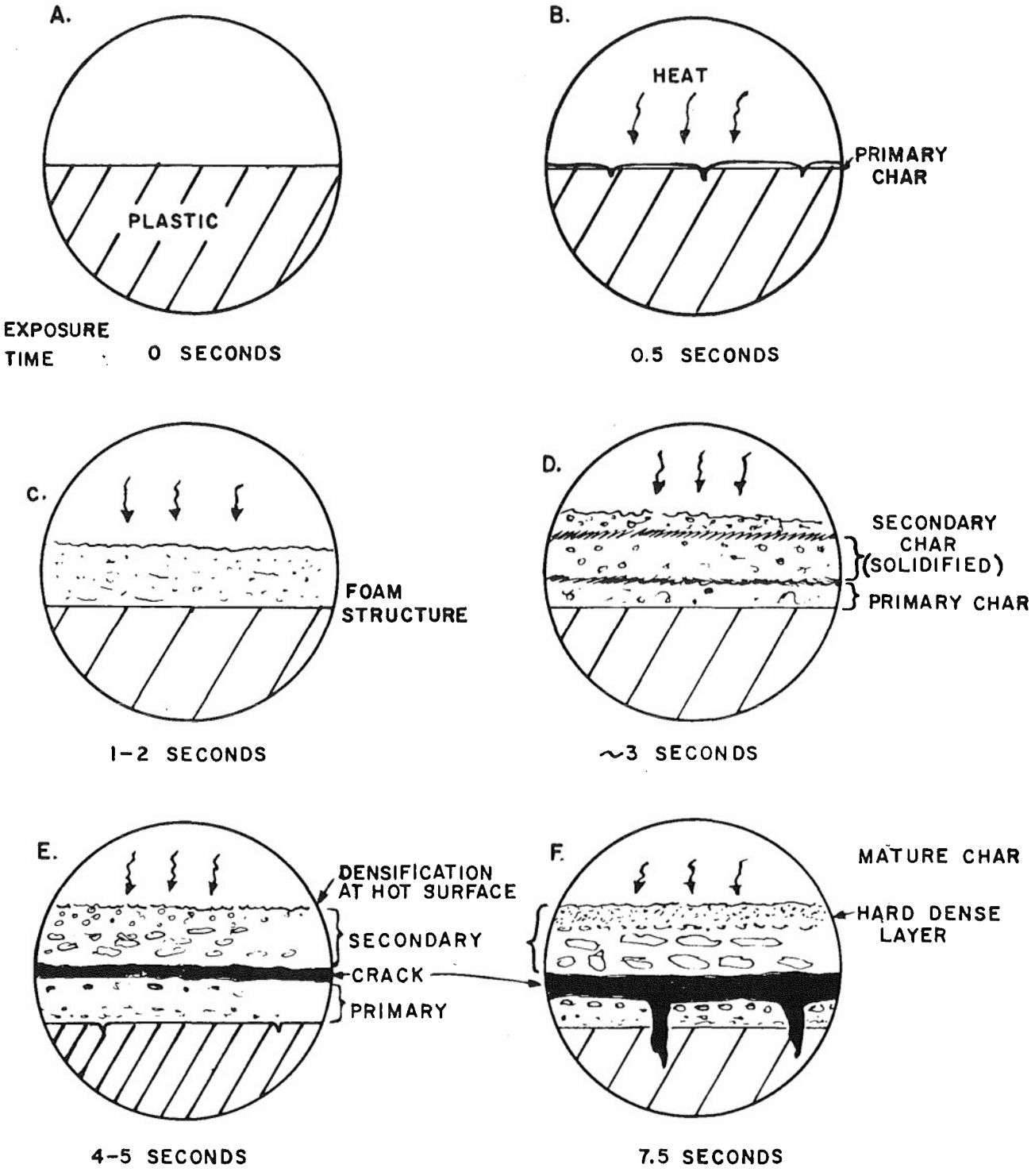

Figure 42. Char Layer Growth of Cast Resin During Ablation

CONCLUDING REMARKS

It has been shown that experimental values of heats of ablation for Teflon agree reasonably well with theoretical predictions for both high and low heating rates. Comparison of the experimental data with theory appears to confirm the trend of a pressure effect on the heat of ablation. Teflon exhibits primarily a steady state response at the stagnation conditions; there are, however, strong non-steady effects evident in the surface temperature, mass loss, backwall temperature data at the skirt region. Quartz as an example of a glassy material which melts, flows, and vaporizes presents an attractive theoretical problem; theoretical predictions of its behavior are in good agreement with experimental data. Graphite suffers little ablation during exposure to a high temperature gas; much of the heat flux penetrates readily into the interior. Material loss occurs by surface oxidation; theoretical predictions depend to a large extent on little known oxidation reactions of the material with the environment, care must be also taken in interpreting data from facilities with significant contamination. Thus, understanding of graphite behavior is not as well founded as that of quartz or Teflon, although reasonable engineering estimates can be made of temperature penetration. The charring plastics, re-inforced or homogeneous, present the most complicated picture. Theories predicting behavior are heavily dependent on experimentally determined parameters. Experimental data indicate a high heat of ablation, due to the formation of a char and the mass transfer gases due to decomposition of the plastic.

The choice of a material for the thermal protection of re-entry vehicles depends to a large extent on the trajectory conditions and engineering considerations. For high heating rates and short time exposure to the hypersonic environment, high Q* materials such as quartz, and charring plastics are attractive. The design of a thermal shield utilizing unmodified graphite is limited by the heat penetration aspects (high backface temperature) rather than by the ablation rate (high Q*) and, therefore, by mechanical limitation as thermal shock and shield fastening problems. Pyrolytic graphite represents an attractive modification. At the low heating rate of long duration characterized by satellite re-entry vehicles, heat penetration characteristics of the material dictate the choice; considerations of non-steady ablation effects are important.

For ablation material experimentation a high enthalpy facility with an uncontaminated air stream is of high priority for all of the materials that are affected by chemistry. This includes most of the material considered with the possible exception of glassy material. As has been noted above, the behavior of graphite and charring materials is not well known in detail. Chemical reactions at the surface, a realistic model accounting for gas "percolation" and subsequent reactions, structural and thermal stress characteristics of the damage layer and base, and the complicated role of reinforcements require further investigation. It would appear that high-purity test facilities (27, 33) are essential to further progress.

Acknowledgement

The contributions of many investigators may be noted from the list of References. The support of the Ballistic Systems Division, Air Force Systems Command, U.S. Air Force, under its Advanced Studies Program, is gratefully acknowledged.

LIST OF SYMBOLS

A	area
B	frequency factor for depolymerization
$C_H(\dot{m})$	Stanton number in the absence of combustion
C_o	concentration of oxygen
C_p	specific heat at constant pressure
d	diameter
E	energy of activation of depolymerization
h	enthalpy
H	gaseous stagnation enthalpy, including chemical enthalpy
ΔH_o	heat of combustion per unit mass of oxygen
ΔH_p	enthalpy change, initial to surface temperature of plastic = $H_{pw}(g) - H_{po}(s) = \int_{T_o}^{T_w} C_{p_p}(s)\,dt \quad \Delta H_v$
ΔH_v	heat of depolymerization per unit volume for plastic; latent heat of vaporization
K	thermal conductivity
ℓ	length
M	molecular weight
m	integrated mass loss per square foot
$\dot{m}$	mass transfer rate (= $\rho_p \dot{x}$ for steady state ablation)
p	pressure
$\dot{q}$	heat transfer rate per square foot
Q	heat transfer rate to surface
Q^*	heat of ablation, = $Q\,(\dot{m} = 0) / \dot{m}_w$
$Q(m = 0)$	heat transfer rate in the absence of mass transfer
Q_p	energy absorbed per unit volume due to pyrolysis
$(\Delta Q/\Delta \dot{m})_w$	change in energy transfer per unit change charge in interphase mass transfer, for no combustion
Q_T	total heat transferred per square foot

R	universal gas constant
R_B	nose radius of the re-entry satellite
r	radius
t	time
T	temperature
ΔT	$T - T_a$
u	tangential velocity, parallel to surface
$\vec{v}$	velocity vector
W	weight
x	coordinate normal to surface, direction into the material
$\dot{x}$	ablation rate
α	thermal diffusivity
α_{vap}	vaporization coefficient
β	stagnation point velocity gradient
Γ	fraction of material ablated which is gaseous
δ	weight depth of test specimen, lb/ft^2 (density of material x length of specimen)
ϵ	total surface emissivity
μ	viscosity
Ξ	fraction of virgin plastic that enters gas phase during surface combustion of char layer
ρ	density

SUBSCRIPTS

a	ablated
Aero	Aerodynamic
B	backwall of test specimen
e	outer edge of gaseous boundary layer, stagnation conditions
f	flight
g	gas
o	initial
p	plastic

q	heating cycle
s	stagnation condition, model
s, pl.	plenum
SG	specific gravity
Sk	skirt region of test specimen
Su	surface of test specimen
t	total
vp	virgin plastic
w	wall
1	small weight depth, stagnation region
2	large weight depth, stagnation region
3	small weight depth, skirt region
4	large weight depth, skirt region
5	weight depth, variable heating test series

REFERENCES

1. Allen, H.J., and Eggers, Jr., A.J., "A Study of the Motion and Aerodynamic Heating of Missiles Entering the Earth's Atmosphere at High Supersonic Speeds", NACA RM A58D28, August 25, 1953

2. Kemp, N.H. and Riddell, F.R., "Re-entry Heat Transfer to Satellite Vehicles", Jet Propulsion, Vol. 27, Part I, February 1957, pp. 132-137

3. Romig, M., "Stagnation Point Heat Transfer for Hypersonic Flight", Jet Propulsion, Vol. 26, No 12, December 1956, pp. 1098-1101 — Addendum, Vol. 27, No. 12, December 1957, p. 1255

4. Scala, S.M., "The Thermal Protection of a Re-entry Satellite", ASME Aviation Conference, Los Angeles, March 9-12, 1959; ARS Journ., Vol. 29, no. 9, September 1959, pp. 670-72

5. Mason, D.J. and Gazley, Jr., C., "Surface Protection and Cooling Systems for High Speed Flight", Aeron, Engineering Review, Vol. 15, no. 11, November 1956, pp. 46-55

6. Sutton, G.W., "The Temperature History in a Thick Skin Subjected to Laminar Heating During Re-entry into the Atmosphere", Jet Propulsion, Vol. 28, No. 1, January 1958, pp. 40-45

7. Sutton, G.W., "The Ablation of Reinforced Plastics in Supersonic Flow", Journal of the Aero/Space Sciences Vol. 27, No. 5, pp. 377-385, May 1960

8. Scala, S.M. and Sutton, G.W., "The Two-Phase Hypersonic Laminar Boundary Layer - A Study of Surface Melting", Proc. 1958 Heat Transfer and Fluid Mechanics Institute, Standford U. Press

9. Bethe, H.H. and Adams, M.C., "A Theory for the Ablation of Glass Materials", J. Aero/Space Sciences, Vol. 27, No. 7, July 1960

10. Lees, L., "Similarity Parameters for Surface Melting of a Blunt Nosed Body in a High Velocity Gas Stream", ARS Journal, Vol. 29, No. 5, May 1959, pp. 345-353

11. Gruntfest, I.J., "Behavior of Reinforced Plastics at Very High Temperatures - Part 2", Modern Plastics, Vol. 36, No. 8, April 1959, pp. 137-148, 204

12. Georgiev, S., Hidalgo, H., and Adams, M., "On Ablation for Recovery of Satellites", AVCO Research Laboratory, Research Report 47, March 6, 1959. 1959 Heat Transfer and Fluid Mechanics Institute, Stanford University Press, pp. 171-180, (June 1959)

13. "Thermal Protection of Structural Propulsion, and Temperature Sensitive Materials for Hypersonic and Space Flight", Chicago Midway Laboratories Data Report CML-DR-M152-2, October 21, 1958

14. Stewart, J.D., "Transpiration Cooling: An Engineering Approach", General Electric Company, Missile and Space Vehicle Department Report - TIS R59SD338, May 1, 1959

15. Friedman, H., "The Mechanism of Polytetrafluoroethylene Pyrolysis", presented at the American Chemistry Society, Atlantic City, N.J. (Sept. 1959)

16. Knuth, E., "Compressible Couette Flow with Diffusion of a Reactive Gas, from a Decomposing Wall", Proc. 1958 Heat Transfer and Fluid Mechanics Institute, Stanford U. Press

17. Sutton, G.W., "Adiabatic Wall Temperature Due to Mass Transfer Cooling With a Combustible Gas", Jet Propulsion, Vol. 29, No. 2 (February 1958), pp. 136-137

18. Sutton, G.W., "Combustion of a Gas Injected into a Hypersonic Laminar Boundary Layer", Proc. Seventh International Combustion Symposium, Butterworths, London, (1958)

19. Goodman, T.R., "The Heat Balance Integral and Its Application to Problems Involving a Change of Phase", Trans. ASME, Vol. 80, No. 2 (February 1958), pp. 335-342

20. Gerstein, M. and Coffin, K.P., "Combustion of Solid Fuels", Combustion Proc., Vol. II High Speed Aerodynamics and Jet Propulsion, Princeton University Press, 1956

21. Scala, S.M., "Surface Combustion in Dissociated Air", Jet Propulsion, Vol. 28, No. 5, May 1958, pp. 340-341

22. Fanucci, J. and Lew, H., "Effect of Mass Transfer and Body Forces on Two Phase Boundary Layer", General Electric Report TIS 59SD380, April 1959

23. Scala, S.M., "Sublimation in a Hypersonic Environment", J. Aerospace Sciences, Vol. 27, No. 1, January 1960

24. Scala, S., "Vaporization of a Refractory Oxide During Hypersonic Flight", 1959 Heat Transfer and Fluid Mechanics Institute, UCLA, June 1959, pp. 181-192 Stanford University Press

25. Scala, S.M. and Vidale, G.L., "Vaporization Processes in the Hypersonic Laminar Boundary Layer", J. of Heat and Mass Transfer, Vol. 1, No. 1, 1960

26. Scala, S. and Baulknight, C., "Transport and Thermodynamic Properties in a Hypersonic Laminar Boundary Layer", Part II, J.A.R.S., Vol. 30, no. 4, 1960

27. Scala, S.M., "A Study of Hypersonic Ablation", Proc. of 10th International Astronautical Congress, Springer-Verlag, Vienna, 1959

28. Warren, W.R., "Laboratory Experimental Studies in Re-entry Aerothermodynamics", Proc. of 10th International Astronautical Congress, Springer-Verlag, Vienna, 1959

29. Ferri, A. and Libby, P.A., "A New Technique for Investigating Heat Transfer and Surface Phenomena under Hypersonic Flow Conditions", J. Aero/Space Sciences, 24, 6, 464, (1959)

30. Diaconis, N., Fanucci, J.B. and Sutton, G.W., "The Heat Protection Potenital of Several Ablation Materials for Satellite and Ballistic Re-entry into the Earth's Atmosphere", Ballistic Missiles and Space Technology, Vol. II, Pergamon Press, 1961

31. Warren, W.R. and Diaconis, N., "The Performance of Ablation Materials as Heat Protection for Re-entering Satellites", GE TIS R60SD316, presented at the Institute of Aero/Space Sciences annual meeting January 1960, IAS paper No. 60-49

32. Steg, L., "Materials for Re-entry Heat Protection of Satellites", Journal ARS, Vol. 30, no. 9, 815, 1961

33. Diaconis, N.S. and Warren, W.R., "Air Arc Simulation of Hypersonic Environments", ARS International Hypersonic Conference, Preprint 1986-61, Aug. 1961

34. Adams, M.C., "Recent Advances in Ablation", Journal American Rocket Society, Vol 29, no. 9, September 1959

35. Lew, H. and Fanucci, J., "A Study of Melting Surfaces", General Electric Co. TIS Report R59SD381, April 1959

36. Scala, S. and Diaconis, N., "Stagnation Point Ablation of Teflon During Hypersonic Flight", Journal of Aero/Space Sciences, Vol. 27, no. 2, February 1960

37. Chen, S. and Allen, S.J., "Similarity Analysis for Transient Melting and Vaporizing Ablation on Blunt Nosed Bodies", American Rocket Society, Preprint 2098-61, October 1961

38. Gilbert, L. and Scala, S., Presented at the ARS meeting October 1961, American Rocket Society, Preprint 2100-61, October 1961

39. Beecher, N. and Rosensweig, "Ablation Mechanisms in Plastics with Inorganic Reinforcement", Journal of American Rocket Society, Vol. 31, no. 4, 532, 1961

40. Adams, M.C., Powers, W.E., and Georgiev, S., "An Experimental and Theoretical Study of Quartz Ablation at the Stagnation Point", Journal Aero/Space Sciences, Vol. 27, no. 7, July 1960

41. Hidalgo, H., "A Theory of Ablation of Glassy Materials for Laminar and Turbulent Heating", Journal ARS, Vol. 30, no. 9, September 1960

42. Georgiev, S., Hidalgo, H. and Adams, M.C., "An Ablation for the Recovery of Satellites", AVCO Everett Research Laboratory, Research Report 65, July 1959

43. Barriault, and Yos, "Analysis of the Ablation of Heat Shield that form a Charred Surface Layer", Journal ARS, Vol. 30, no. 9, 823, September 1960

44. Wachman, H.Y., Linevsky, M.J., and McGinn, J.H., "The Effects of Electrode Contamination on the Properties of Air-Arc Plasmas", Proc. of Fourth Symposium of Advances in Ballistic Missile and Space Technology, Vol. 2, pp. 374-381, Pergamon Press, New York, 1961

45. Wachman, H.Y., and Linevsky, M.J., "Equilibrium Chemical Composition and Therodynamic Properties of Carbon-Contaminated Oxygen Enriched Air at High Temperatures", General Electric Report TIS R60SD418, May 1960

46. Wachman, H.Y., and Linevsky, M., "The Chemical Composition and Thermodynamic Properties of Air Carbon Mixtures", General Electric Report TIS No. R59SD349, 1959

47. McGinn, J.H., "A New Type Arc for Producing High Temperature, High Purity Plasma Jets", 5th Inter. Conference on Ionization Phenomena in Gases, Munich, Germany, August 1961

48. Scala, S.M., and Nolan, E.J., "Aero Thermodynamic Feasibility of Graphite for Hypersonic Glide Vehicles," Proceedings of the 5th BMD/STL Symposium on Ballistic Missile and Space Technology, Vol. 4, pp. 31-63, August 1960

49. Denison, M.R., "The Turbulent Boundary Layer on Chemically Active Ablating Surface; Journal Aero/Space Sciences 28, 6, June 1961

50. Scala, S.M., "The Ablation of Graphite in Dissociated Air", (to be published)

51. Blecker, S. and Sutton, G.W., "Comparison of Some Approximate Method for Calculating Re-entry Ablation of a Subliming Material", Journal ARS Vol. 31, no. 3, March 1961

52. Barry, W.T. and Sutton, W.H., "The Importance of Char Structure in the Ablation Performance of Organic Polymers", General Electric TIS R60SD329, 1960

53. Adams, E., "Theoretical Investigation of the Ablation of a Glass Type Heat Protection Shield of Varied Material Properties at the Stagnation Point of a Re-entering IRBM", NAS A TND-564, January 1961

GENERAL ELECTRIC

SPACE SCIENCES LABORATORY
MISSILE AND SPACE VEHICLE DEPARTMENT

TECHNICAL INFORMATION SERIES

AUTHOR	SUBJECT CLASSIFICATION	NO.
L. Steg H. Lew	Materials, Ablating	R62SD55
		DATE May, 1962

TITLE

HYPERSONIC ABLATION

ABSTRACT

The severe high enthalpy environment generated by vehicles entering into atmospheres at hypersonic speeds has led to the consideration of material ablation as a means of alleviating the high heat flux. This survey paper reviews four classes of materials:

1. Plastics which depolymerize to a gas but do not liquefy.
2. Materials which sublime and react with the constituents of dissociated air.
3. Materials which first melt and then vaporize.
4. Composite materials which pyrolyze and char.

The behavior of these materials is discussed from experimental and theoretical points of view, and some interesting areas for further investigation are pointed out.

G. E. CLASS	REPRODUCIBLE COPY FILED AT	NO. PAGES
I	G. E. TECHNICAL INFORMATION CENTER 3198 CHESTNUT STREET PHILADELPHIA, PENNA.	61
GOV. CLASS None		

By cutting out this rectangle and folding on the center line, the above information can be fitted into a standard card file.

AUTHOR _____

COUNTERSIGNED _____

DIVISION Defense Electronics

LOCATION Valley Forge Space Technology Center, King of Prussia, Pa.